8474–8489 *Nucleic Acids Research, 2020, Vol. 48, No. 15* *Published online 11 July 2020*
doi: 10.1093/nar/gkaa587

Dual roles of yeast Rad51 N-terminal domain in repairing DNA double-strand breaks

Tai-Ting Woo[1], Chi-Ning Chuang[1], Mika Higashide[2], Akira Shinohara[2] and Ting-Fang Wang[1,*]

[1]Institute of Molecular Biology, Academia Sinica, Taipei 115, Taiwan and [2]Laboratory of Genome-Chromosome Functions, Institute for Protein Research, Osaka University, 3-2 Yamadaoka, Suita, Japan

Received October 22, 2019; Revised June 24, 2020; Editorial Decision June 25, 2020; Accepted July 03, 2020

ABSTRACT

Highly toxic DNA double-strand breaks (DSBs) readily trigger the DNA damage response (DDR) in cells, which delays cell cycle progression to ensure proper DSB repair. In *Saccharomyces cerevisiae*, mitotic S phase (20–30 min) is lengthened upon DNA damage. During meiosis, Spo11-induced DSB onset and repair lasts up to 5 h. We report that the NH_2-terminal domain (NTD; residues 1–66) of Rad51 has dual functions for repairing DSBs during vegetative growth and meiosis. Firstly, Rad51-NTD exhibits autonomous expression-enhancing activity for high-level production of native Rad51 and when fused to exogenous β-galactosidase *in vivo*. Secondly, Rad51-NTD is an S/T-Q cluster domain (SCD) harboring three putative Mec1/Tel1 target sites. Mec1/Tel1-dependent phosphorylation antagonizes the proteasomal degradation pathway, increasing the half-life of Rad51 from ∼30 min to ≥180 min. Our results evidence a direct link between homologous recombination and DDR modulated by Rad51 homeostasis.

INTRODUCTION

RecA-like DNA recombinases are the central enzymes responsible for catalyzing the strand exchange reaction during homology-directed repair and recombination (HDRR). This error-free and template-dependent pathway repairs DNA double-strand breaks (DSBs) produced by collapse of replication forks, thereby upholding genome integrity (1,2). HDRR is also responsible for the repair of Spo11-induced DSBs during meiotic prophase (3,4). Most eukaryotic organisms possess two RecA-like recombinases, Rad51 and Dmc1. Rad51 is ubiquitously found in all eukaryotic cells, whereas Dmc1 is meiosis-specific (5). In *Saccharomyces cerevisiae* yeast, both Rad51 and Dmc1 are required for meiosis (6,7). However, the catalytic function of Rad51 is inhibited by direct interaction with a meiosis-specific protein, Hed1 (8), which renders Rad51 an accessory factor to Dmc1 during meiosis (9). It was also reported previously that Dmc1-mediated recombination is more efficient than Rad51-mediated recombination in meiosis of diploid hybrid yeasts (e.g. SK1/S288c and YJM/S288c) (10), given that the homologous chromosomes are highly polymorphic and Dmc1 is superior to Rad51 in tolerating mismatched sequences during their strand exchange reaction (11,12).

DSBs are one of the most deleterious and harmful DNA lesions. Repair of DSBs in eukaryotes is monitored by the DNA damage response (DDR), which operates similarly during mitosis and meiosis (13). ATM (ataxia-telangiectasia mutated) and ATR (RAD3-related) are the upstream sensor kinases that phosphorylate mammalian target proteins during DDR (14–16). Mec1 and Tel1 are the *S. cerevisiae* orthologs of mammalian ATR and ATM, respectively (17). ATR^{Mec1} and ATM^{Tel1} preferentially phosphorylate serines (S) and threonines (T) that are followed by glutamine (Q) (18). A large number of $Mec1^{ATR}$ and $Tel1^{ATM}$ targets contain at least one S/T-Q cluster domain (SCD), which has been defined as the presence of at least three S/T-Q sites in a stretch of 50 amino acids in *S. cerevisiae* or 100 amino acids in mammals (19,20). During yeast mitosis, $Tel1^{ATM}$ and $Mec1^{ATR}$ phosphorylate the Rad9 adaptor protein, which in turn activates Rad53 kinase (the yeast ortholog of CHK2) for DDR signaling (21). Rad53 amplifies the signaling cascade by phosphorylating another kinase, Dun1 (22,23).

During *S. cerevisiae* meiosis, $Tel1^{ATM}$ and $Mec1^{ATR}$ phosphorylate the SCD (residues 258–324) of Hop1, a Rad53-like chromosomal adaptor protein, particularly at the $T^{318}Q$ motif. Hop1 phosphorylation promotes its binding to the forkhead-associated (FHA) domain of Mek1, a meiosis-specific CHK2-like kinase, leading to activation of Mek1 (24,25). The Hop1–Mek1 interaction is similar to that of the Rad9–Rad53 and Rad53–Dun1 signaling pathways, which are mediated through the interaction of phosphorylated Rad9–SCD with Rad53–FHA and phosphorylated Rad53–SCD1 with Dun1–FHA, respectively (25,26). Subsequently, Mek1 promotes homolog bias via inhibition

*To whom correspondence should be addressed. Tel: +886 2 27899188; Email: tfwang@gate.sinica.edu.tw

of Rad51 by: (i) phosphorylating and stabilizing Hed1, the meiosis-specific inhibitor of Rad51 and (ii) also phosphorylating the Rad51 accessory factor Rad54, leading to a reduced binding affinity of Rad54 for Rad51 (8,10,27,28).

Hop1 is not the only substrate that is phosphorylated by Tel1^{ATM} and Mec1^{ATR} during yeast meiosis. These two protein kinases sequentially phosphorylate several other protein targets during meiotic prophase, including γH2A (29), Zip1 (the transverse filament of the synaptonemal complex, SC) (30), Rec114 (an accessory factor of Spo11) (31), Sae2 (an endonuclease for DSB resection) (32) and RPA (a single-stranded DNA binding protein complex) (33). Also noteworthy is that Mec1^{ATR}- and Tel1^{ATM}-dependent γH2A phosphorylation emerges at the onset of premeiotic S phase and, therefore, it is independent of Spo11 (i.e. initiation of meiotic DSBs) and Red1, a meiosis-specific axial-element protein. Mec1^{ATR}- and Tel1^{ATM}-dependent Zip1 phosphorylation requires Spo11 but not Red1, whereas Mec1^{ATR}- and Tel1^{ATM}-dependent Hop1 phosphorylation requires both Spo11 and Red1 (34). Pachytene checkpoint protein 2 (Pch2) specifically prevents Red1-independent Hop1 phosphorylation (35). It has also been reported that Pch2 is involved in the initiation of Spo11-induced DSBs, with DSBs being reduced further when a *pch2*Δ mutant is combined with a hypomorphic allele of *SPO11* (36). Alternatively, Pch2 might act together with Tel1^{ATM} to control the resection and interhomolog process during early meiosis when DSB levels are low. When the levels of genome-wide DSBs reach a certain threshold, Mec1^{ATR} takes over control and progressively strengthens the homolog bias (37).

Mec1^{ATR} also has an essential function in regulating protein homeostasis in *S. cerevisiae* (38,39), but it is still unclear which Mec1^{ATR} targets are involved in this intriguing function. In this study, we report that Tel1^{ATM} and Mec1^{ATR} phosphorylate the SCD (1–66 residues) of *S. cerevisiae* Rad51 recombinase to protect Rad51 recombinase from proteasome-mediated degradation. We also show that Rad51-NTD exhibits a novel function in promoting high steady-state levels of Rad51 during both vegetative growth and meiosis.

MATERIALS AND METHODS

Yeast strains and two-hybrid assay

All meiotic experiments were performed using diploid isogenic SK1 strains. Plasmids are listed in Supplementary Table S1, and genotypes of strains are described in Supplementary Table S2. Quantitative yeast two-hybrid assays, tetrad dissection, immunostaining of chromosome spreads, cycloheximide-shutoff experiments, and physical analyses were carried out as previously described (10,40–43).

Antisera, immunoblotting and cytology

Rabbit antisera against phosphorylated Rad51-S^{2}Q, Rad51-S^{12}Q, Rad51-S^{30}Q and Rad51-S^{192}Q were raised using the synthetic phosphopeptides M^{1}S$^{[P]}$QVQEQHISESQL^{14}, E^{6}QHI SES$^{[P]}$QLQYGNGS^{20}, T^{24}VPADLS$^{[P]}$QSVVDGNGN^{39} and E^{182}LFGEFRTGKS$^{[P]}$QLCHT^{197} as antigens, respectively, where S$^{[P]}$ is phosphorylated serine. The antisera were pre-cleaned by peptide-specific affinity chromatography using the corresponding non-phosphorylated peptides coupled to agarose beads. Phosphopeptide synthesis and animal immunization were conducted by LTK BioLaboratories, Taiwan. The rabbit antisera against Hop1, rabbit antisera against phosphorylated Hop1-T^{318}Q and the goat antisera against Zip1 were described previously (25). The goat anti-Rad51 antibody (yN-19), goat anti-Clb1 antibody (yS-19) and rabbit anti-Sic1 antibody (FL-284) for western blot were purchased from Santa Cruz Biotechnology (CA, USA). The rabbit anti-Dmc1 antibody was a gift from Douglas Bishop (University of Chicago, IL, USA). The rat anti-HA antibody was purchased from Roche (Basel, Switzerland). The mouse anti-V5 antibody was purchased from Bio-Rad (CA, USA). The rabbit anti-Hsp104 and anti-hexokinase antisera were kindly provided by Chung Wang (Academia Sinica, Taiwan). The phospho-specific Rad51-S^{192}Q antiserum (44) was a gift from Stephen Jackson (University of Cambridge, UK). Western blotting analyses were performed as described (41). The protein signals on Western blot membranes were exposed to X-ray films (Fujifilm Medical, Tokyo, Japan) or visualized and captured using ImageQuant LAS 4000 (GE Healthcare, IL, USA) and quantified using ImageJ (NIH, MD, USA). Cytological analyses using rabbit anti-Dmc1 and guinea pig anti-Rad51 were carried out as previously described (43). Stained samples were observed using an epi-fluorescent microscope (BX53, Olympus) with a 100X objective (NA1.4). Images were captured by a CCD camera (CoolSNAP HQ2, Teledyne Photometrics) at room temperature, and then processed using iVision software (BioVision Technologies).

Dephosphorylation assay

Bovine intestinal alkaline phosphatase (Sigma-Aldrich) was used for *in vitro* protein dephosphorylation reactions following the manufacturer's instructions. In brief, whole-cell extracts of ∼6 × 10^{7} yeast cells precipitated with trichloroacetic acid (TCA, Sigma-Aldrich) were dissolved in 150 μl of phosphatase reaction buffer (5 mM Tris–HCl pH 8.0, 10 mM NaCl, 1 mM $MgCl_2$ and 0.1 mM dithiothreitol), and then 3–4 μl of 2 M Tris–Base was added to adjust the pH to 7.9. Dephosphorylation reactions were carried out by mixing 37.5 μl of whole-cell extracts with 100 U of bovine intestinal alkaline phosphatase, followed by incubation for 4 h at 30°C. In the negative control experiments, the phosphatase inhibitor 2-glycerophosphate (Sigma-Aldrich) was added to a final concentration of 16 μM. Dephosphorylation reactions were stopped by the addition of 7% TCA for the subsequent precipitation. The pellet was resuspended in protein sample buffer and then incubated for 10 min at 65°C before analyses using SDS polyacrylamide gel electrophoresis.

RESULTS

The NH_2-terminal domain (NTD) of *S. cerevisiae* Rad51 is critical for binding to Hed1

It was previously reported that the Rad51-interacting motif of Hed1 is a narrow region spanning amino acid residues

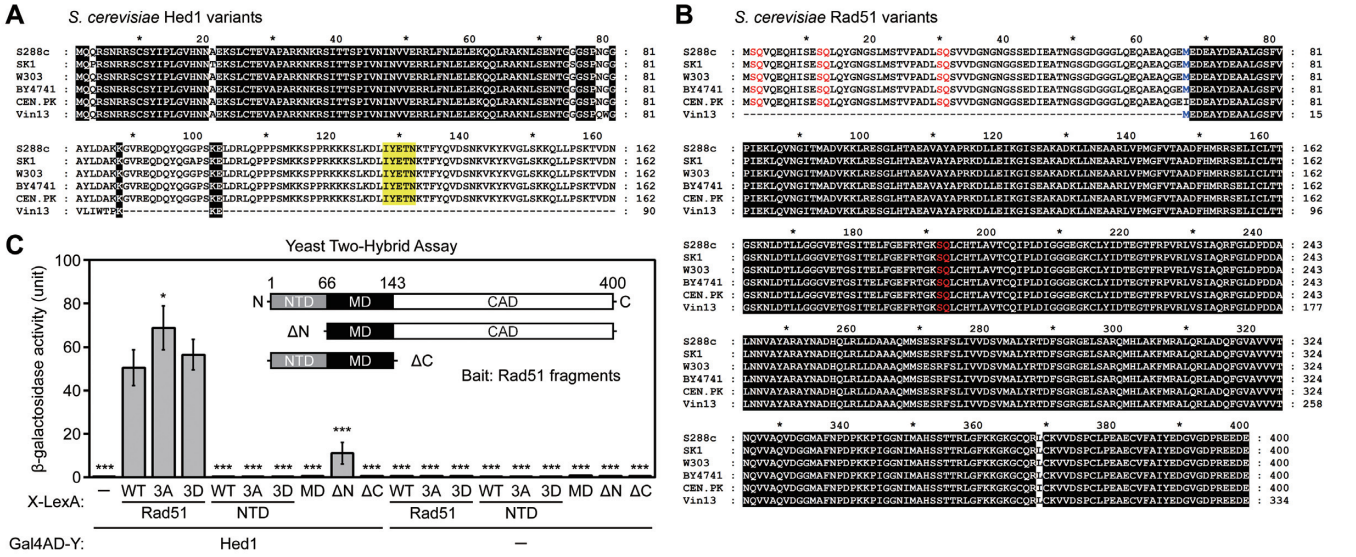

Figure 1. Interactions of Rad51 and Hed1 proteins. Sequence comparison of Hed1 and Rad51 in different yeast strains reveals loss of the COOH-terminal region of Hed1 (**A**), and the NH_2-terminal region of Rad51 (**B**) in the budding yeast strain Vin13. Protein sequences were retrieved from the *Saccharomyces* Genome Database (SGD). Multiple sequence alignments were performed with MAFFT version 7 (63), and the results were displayed and edited with GeneDoc (version 2.7.000; https://www.softpedia.com/get/Science-CAD/GeneDoc.shtml). Identical residues are shaded in black. (**A**) The reported Rad51-interacting region of Hed1 is shaded in yellow. (**B**) The initial 66 amino acid stretch (Met^1 to Glu^{66}) of *S. cerevisiae* Rad51 is defined as the NH_2-terminal domain (NTD). Three SQ motifs (S^2Q, $S^{12}Q$ and $S^{30}Q$) in the NTD and one $S^{192}Q$ motif in the ATPase domain are highlighted in red. The methionine (Met^{67}) following the NTD is shown in blue. (**C**) Yeast two-hybrid assay showing interactions between Rad51 fragments and Hed1. Quantitative yeast LacZ assays were performed as described previously (40,41). Hed1 is expressed from pGADT7 vectors (Clontech, USA), whereas in X-LexA the bait protein X is NH_2-terminal to LexA (64) (Supplementary Table S3). Error bars indicate standard deviation between experiments ($n \geq 3$, see Supplementary Table S3 for the exact sample sizes). Asterisks indicate significant differences when compared to values of interaction between WT Rad51–LexA and Gal4AD–Hed1, with P values calculated using a two-tailed t-test (*P value < 0.05 and ***P value < 0.001).

128–132, based on yeast two-hybrid (Y2H) assay (27). A homology search using NCBI BLAST revealed that Hed1 and the NTD of Rad51 (Supplementary Figure S1) are specific to the genus *Saccharomyces*. Multiple sequence alignments further revealed that both Rad51-NTD and the Rad51-interacting domain of Hed1 have been concomitantly lost in the wine-making strain Vin13 (Figure 1A and B). Vin13 was originally obtained by hybridizing *S. bayanus* and *S. cerevisiae* (http://www.scottlabsltd.com/product/vin-13-premium-yeast/).

The results of quantitative yeast two-hybrid assay (41) revealed that Rad51-ΔN, an NTD truncation mutant (residues 67–400), exhibited much weaker Y2H interactions with Hed1 than wild-type (WT), whereas the NTD alone (residues 1–66), the middle domain (MD; residues 67–143), and the CAD truncation mutant (ΔCAD; residues 1–143) were each incapable of Hed1 interaction (Figure 1C and Supplementary Table S3). The results of our immunoblotting experiments indicate that all Rad51 fragments were well expressed in the *rad51*Δ Y2H reporter cells (Supplementary Figure S2). We conclude that NTD is important but dispensable for the binding of Rad51 to Hed1.

Rad51-NTD itself has profound impacts for repairing DSBs during both vegetative growth and meiosis

To further examine the functional importance of Rad51-NTD *in vivo*, we generated both haploid and diploid *rad51-ΔN* mutants that express the Rad51-ΔN proteins under the control of the native *RAD51* promoter. The *rad51-ΔN* diploid cells displayed ∼50% reduction in spore viability (Table 1). When vegetative cells were exposed to the DNA damaging agent methyl methanesulfonate (MMS), the *rad51-ΔN* haploid mutant, unlike *rad51*Δ, grew similarly to wild-type cells on YPD plates (complete media) with or without 0.01% (w/v) MMS (Figure 2A). However, the *rad51-ΔN* mutant displayed lower viability on YPD plates with 0.02% MMS. These results indicate that Rad51-ΔN possesses (at least in part) the capability to promote HDRR during both mitosis and meiosis, but with lower efficiency (Figure 2A and Table 1).

Immunoblotting time-course experiments further revealed that the steady-state Rad51-ΔN protein levels in *rad51-ΔN* cells were much lower than those of Rad51 protein in WT cells during vegetative growth (Figure 3A and B) or meiosis (Supplementary Figure S3A). Under vegetative conditions and upon MMS treatment to induce expression of Rad51 protein in WT, the steady-state level of Rad51-ΔN protein in *rad51-ΔN* cells was only ∼3% relative to that of Rad51 in WT (Figure 3C). In addition, *rad51-ΔN* sporulating cells exhibited a delayed meiotic progression (Figure 4A).

Deficiency of the meiotic-specific recombinase Dmc1 (i.e. *dmc1*Δ) results in a very strong meiotic progression arrest phenotype at prophase I (MI arrest, Figure 4A) (7). However, both sporulation and spore viability are greatly improved in a *dmc1*Δ *hed1*Δ mutant, presumably due to valid interhomolog recombination being conducted by Rad51 in the absence of the inhibitory effects exerted by Hed1 (8). Like *dmc1*Δ, the *dmc1*Δ *rad51-ΔN* meiotic cells

Table 1. Spore viability

Strain	Spore viability[a]	Tetrad class (viable: non-viable)				
		4:0	3:1	2:2	1:3	0:4
RAD51	97% ($n = 152$)	92%	5%	3%	0%	0%
*rad51*Δ	0% ($n = 100$)	0%	0%	0%	0%	100%
rad51-ΔN	51% ($n = 216$)	7%	30%	28%	28%	7%
*rad51-ΔN sml1*Δ	83% ($n = 144$)	42%	53%	3%	3%	0%
rad51-S2A	99% ($n = 216$)	98%	0%	2%	0%	0%
rad51-S12A	100% ($n = 216$)	100%	0%	0%	0%	0%
rad51-S30A	100% ($n = 216$)	98%	2%	0%	0%	0%
rad51-S2A S12A	100% ($n = 216$)	98%	2%	0%	0%	0%
rad51-3A	97% ($n = 216$)	94%	2%	2%	0%	2%
rad51-3D	97% ($n = 288$)	96%	2%	0%	0%	2%
*dmc1*Δ *hed1*Δ	74% ($n = 216$)	61%	2%	20%	6%	11%
*rad51-3A dmc1*Δ	No spore	—	—	—	—	—
*rad51-3D dmc1*Δ	No spore	—	—	—	—	—
*rad51-ΔN dmc1*Δ	No spore	—	—	—	—	—
*rad51-3A dmc1*Δ *hed1*Δ	No spore	—	—	—	—	—
*rad51-3D dmc1*Δ *hed1*Δ	70% ($n = 220$)	53%	4%	27%	4%	13%
*rad51-ΔN dmc1*Δ *hed1*Δ	No spore	—	—	—	—	—
*mec1-kd sml1*Δ *dmc1*Δ *hed1*Δ	7% ($n = 216$)	2%	2%	6%	4%	87%

[a]Spore viability was analyzed after 3 days on sporulation media at 30°C. To score spore viability, only tetrads (but not dyads or triads) were dissected on YPD.

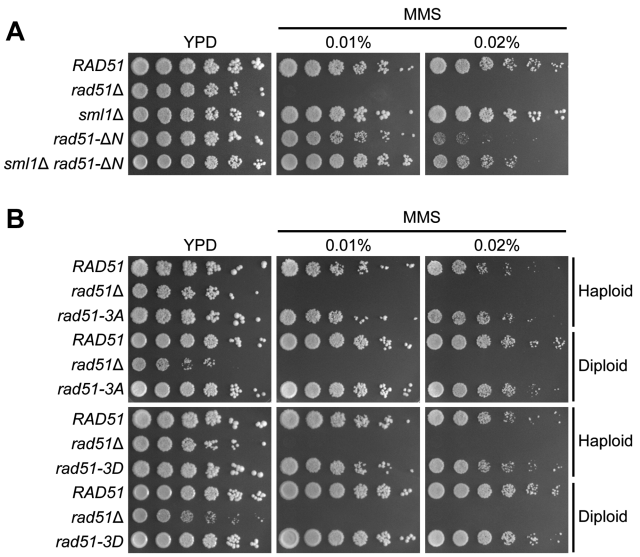

Figure 2. Rad51-NTD itself is more important than Rad51-NTD phosphorylation for HDRR in vegetative cells exposed to excessive DNA damaging agents. Spot assay showing five-fold serial dilutions of yeast strains grown on YPD plates with or without MMS at the indicated concentrations (w/v). (**A**) Analysis of haploid yeast strains, with genotypes indicated at left. (**B**) Analysis of both haploid and diploid yeast strains. Ploidy of the different strains is indicated at right.

hardly formed any spores (Table 1). We speculate that this sever defect could be due to the extremely low protein levels of Rad51-ΔN when the other recombinase, i.e. Dmc1, is absent. It is also possible that the residual activity of Rad51-ΔN is further suppressed by Hed1 during the *dmc1*Δ *rad51-ΔN* meiosis since that our Y2H results suggest that Rad51-NTD is not the only structural region in Rad51 that mediates Rad51–Hed1 interactions (Figure 1C).

Interestingly, removal of the *SML1* gene, which encodes an inhibitor of ribonucleotide reductase (45), could partially suppress the hypersensitivity of the *rad51-ΔN* mutant to excessive DNA damaging agents (0.02% MMS) during vegetative growth (Figure 2A) and increased its spore viability (Table 1). The *sml1*Δ null mutant is a suppressor of mutations of DDR checkpoint kinases, e.g. *mec1-kd* (kinase dead) and *rad53*Δ (46). Also noteworthy is that introducing the *sml1*Δ allele into the *rad51-ΔN* mutant did not significantly increase the steady-state protein levels of Rad51-ΔN (Figure 3B). These results suggest that Rad51-NTD might be functionally linked to the DNA damage checkpoint. Rad51-NTD has three SQ motifs ($S^{2}Q$, $S^{12}Q$ and $S^{30}Q$) (Figure 1B). This clustering of three SQ motifs within a stretch of 30 amino acids fulfills the criteria to define an SCD (20). One intriguing possibility is that Rad51-NTD might be phosphorylated in response to a DNA damage checkpoint.

Rad51-NTD is phosphorylated in a $Mec1^{ATR}$- and $Tel1^{ATM}$-dependent manner during vegetative growth and meiosis

To examine the hypothesis that the three SQ motifs in Rad51-NTD are phosphorylated in DDR, we generated antisera specific to the phosphorylated Rad51-$S^{2}Q$, Rad51-$S^{12}Q$ and Rad51-$S^{30}Q$ peptides (see 'Materials and Methods' section). The specificity of these antisera was validated by immunoblotting experiments following protein dephosphorylation assay (Supplementary Figure S4) as well as immunoblotting experiments using yeast strains carrying different mutant alleles. The *rad51-S2A*, *rad51-S12A* and *rad51-S30A* variants each encodes a respective mutant protein in which the Rad51 serine residue has been mutated into alanine. In the phosphorylation-defective mutant (*rad51-3A*), all three of these serine residues were mutated into alanines. All three SQ motifs in Rad51-NTD were phosphorylated in a $Mec1^{ATR}$- and $Tel1^{ATM}$-dependent manner in vegetative cells exposed to MMS, as well as during normal meiosis (Figure 3D-F). No or negligible signals of corresponding antisera were detected in the three single-amino-

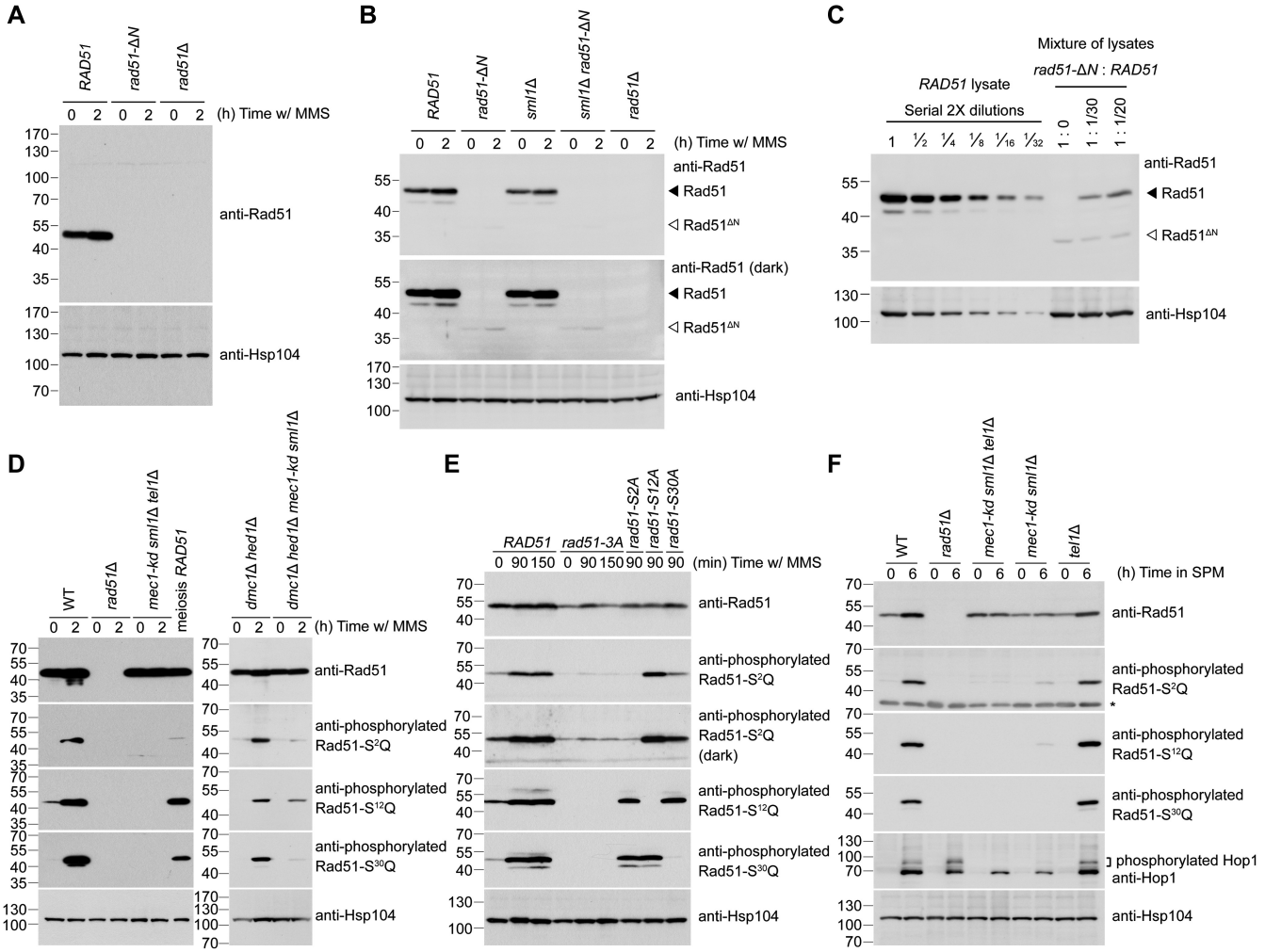

Figure 3. Reduction of steady-state protein levels of Rad51-ΔN and the Mec1^{ATR}- and Tel1^{ATM}-dependent phosphorylation of Rad51-NTD. Total cell lysates were prepared from mitotic cells under MMS treatment (**A-E**), or from meiotic cells at indicated time-points after being transferred into sporulation media (SPM) (**F**), and then visualized by immunoblotting with the corresponding antisera. The asterisk indicates non-specific bands. Hsp104 was used as a loading control. Size in kilodaltons of standard protein markers is labeled to the left of the blots. (**A**) Absence of the NTD from Rad51-ΔN protein was confirmed by immunoblotting using goat anti-Rad51 antibody (yN-19) purchased from Santa Cruz Biotechnology (CA, USA). This antibody (sc-8936) was generated using a peptide mapping at the N-terminus of yeast Rad51. (**B, C**) Immunoblotting using guinea pig anti-Rad51 antisera that recognize the whole Rad51 protein (43), as depicted in Supplementary Figure S2A. The predicted molecular weight of Rad51-ΔN is 36,270 daltons, marked by white arrowheads to the right of the blots. Black arrowheads represent wild-type Rad51 at 42,944 daltons. (**C**) Total cell lysates from wild-type (WT) mitotic cells under MMS treatment were diluted with those of *rad51-ΔN* or empty sample buffer at indicated titers to estimate the relative steady-state protein levels of WT Rad51 and Rad51-ΔN. (**E**) Demonstration of the specificity of anti-phosphorylated Rad51-S^{2}Q, Rad51-S^{12}Q and Rad51-S^{30}Q antisera. The darker exposure (third panel from top) illustrates that the phosphorylation-defective mutant proteins (Rad51-3A and Rad51-S2A) were slightly recognized by anti-phosphorylated Rad51-S^{2}Q antisera.

acid substitution mutants (i.e. *rad51-S2A*, *rad51-S12A* or *rad51-S30A*), the phosphorylation-defective mutant *rad51-3A* (Figure 3E), or the *mec1-kd sml1Δ tel1Δ* triple mutants (Figure 3D and F). To elucidate which kinase is more important for phosphorylation activity, we carried out immunoblotting using cell lysates collected from meiotic cultures of the *tel1Δ* single mutant and the *mec1-kd sml1Δ* double mutant. Consistent with phosphorylation of Hop1 (detected as the slower migrating species in immunoblots) being greatly reduced in the *mec1-kd sml1Δ* strain during meiosis (24,25), we found that all three SQ motifs in Rad51-NTD showed dramatically reduced phosphorylation signals in the *mec1-kd sml1Δ* double mutant, whereas mutation of *tel1Δ* did not induce such an apparent effect (Figure 3F). These results suggest that Mec1^{ATR} plays a more prominent role than Tel1^{ATM} in Rad51-NTD phosphorylation during meiosis.

Rad51-NTD phosphorylation is not strictly dependent on *SPO11*, but is regulated by meiotic DSB levels

In respect of the DNA damage checkpoint-dependent phosphorylation of Rad51-NTD, we examined if Rad51-NTD phosphorylation during meiosis is Spo11-dependent using the phospho-specific Rad51-S^{12}Q antisera. Meiosis of the mutant strains carrying *spo11-da-HA,* i.e. the hypomorphic

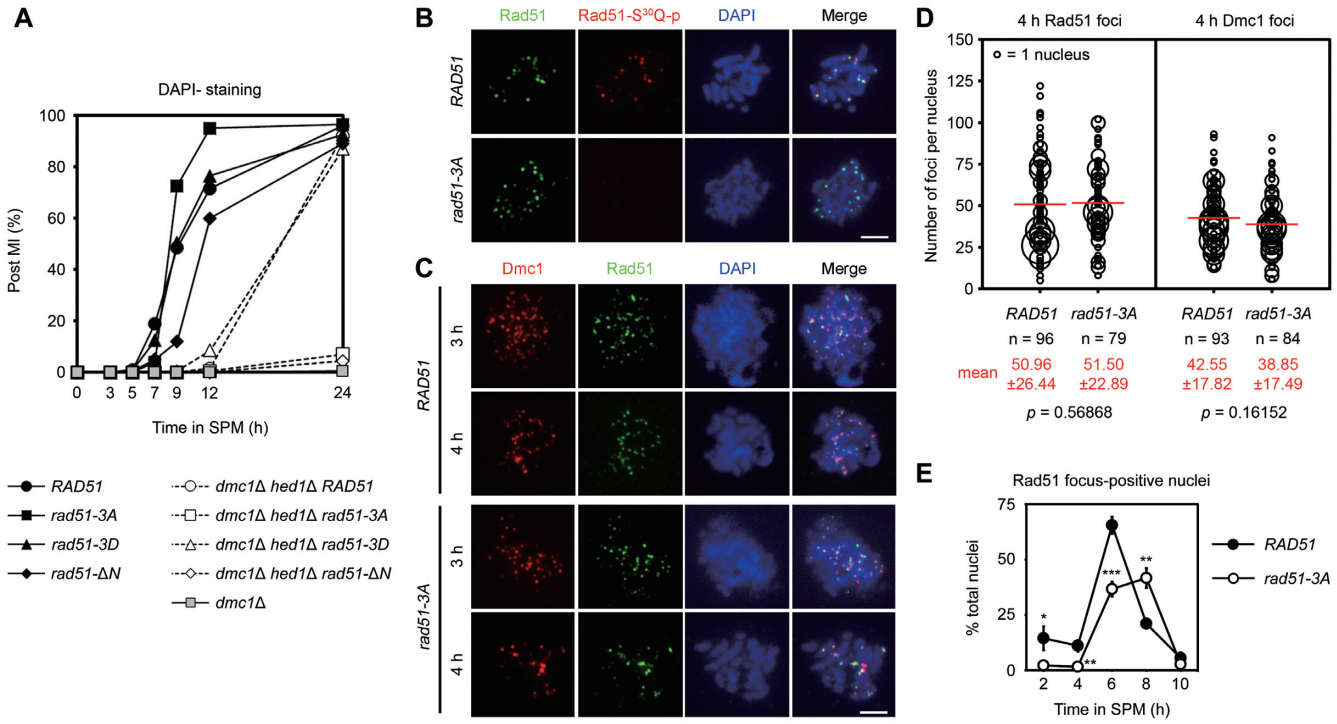

Figure 4. Rad51-NTD and its phosphorylation are indispensable for Rad51-only meiotic recombination during *dmc1*Δ *hed1*Δ meiosis. (**A**) Meiotic progression was monitored by DAPI (4′,6-diamidino-2-phenylindole)-staining of nuclei. Cells harvested from SPM having two or four nuclei (as determined by fluorescence microscopy) were assessed as having completed meiosis I (MI), and the percentage of such cells over total cells counted ($n = 200$) per time-point was plotted. (**B**, **C**) Cytology. Representative images of meiotic nuclear surface spreading experiments using guinea pig anti-Rad51 (green) and anti-phosphorylated Rad51-S^{30}Q (red) or anti-Dmc1 (red) antisera, respectively. Meiotic chromosomes were stained with DAPI (blue) at indicated sporulation time-points. Scale bars, 5 μm. (**D**) Quantification of the numbers of Rad51 and Dmc1 foci in the WT and *rad51-3A* strains. The numbers of foci in each foci-positive chromosome spread (with more than five foci) were counted and plotted as shown. The sizes of circles are proportional to the numbers of nuclei with a given number of foci. The mean number of foci per nucleus is shown in red (bottom), and also as a red bar in the graph. Standard deviations of numbers of foci are shown in parentheses. *n* represents the number of nuclei analyzed for foci-counting. The *P* values were calculated using a two-tailed Mann–Whitney's *U*-test. (**E**) Kinetics of Rad51 foci in meiosis of WT and *rad51-3A* strains. For each replicate of experiments ($n = 3$), Rad51-foci-positive nuclei (with more than five foci) were examined in 60 chromosome spreads. Error bars indicate standard deviation between experiments. Asterisks indicate significant difference between WT and *rad51-3A* strains, with *P* values calculated using a two-tailed *t*-test (*P value < 0.05; **P value < 0.01 and ***P value < 0.001).

allele of *SPO11* resulting in ∼80% reduction of DSB formation, was used for comparison (47). Our meiotic time-course immunoblotting experiments revealed that Hop1-T^{318}Q phosphorylation did not occur in the *spo11*Δ strain and it was greatly reduced in the *spo11-da-HA* strain relative to WT (Supplementary Figure S5A and B). In contrast, Rad51-S^{12}Q phosphorylation remained detectable in the *spo11*Δ strain at a reduced level (∼29% compared to the maximum intensity in WT), but it was largely diminished in the *mec1-kd sml1*Δ *tel1*Δ triple mutants (Supplementary Figure S5A). Moreover, phosphorylation of Rad51-S^{12}Q was reduced by ∼50% during meiosis of the *spo11-da-HA* strain (Supplementary Figure S5B, second panel from top), whereas protein levels of Hop1, Dmc1 or Rad51 were not obviously perturbed.

It was suggested previously that *pch2*Δ mutation and hypomorphic *spo11* reduce DSB formation through distinct mechanisms, with DSB formation being further reduced upon combining these two mutations (36). Consistently, we found that the *pch2*Δ mutation did not affect Hop1-T^{318}Q phosphorylation or Rad51-S^{12}Q phosphorylation in the *SPO11* strain (Supplementary Figure S5B). However, unlike Rad51-S^{12}Q phosphorylation, Hop1-T^{318}Q phosphorylation was more profoundly reduced in the *pch2*Δ *spo11-da-HA* double mutant (Supplementary Figure S5B, second panel from bottom). We conclude that phosphorylation of Hop1 and Rad51-NTD in meiosis is differentially regulated; both types of phosphorylation require Mec1^{ATR} and Tel1^{ATM}, but only Rad51-NTD phosphorylation can occur when cellular DSB levels are very low, even in the absence of *SPO11*. This outcome is not surprising given that Mec1^{ATR}- and Tel1^{ATM}-dependent Rad51-NTD phosphorylation also occurs during vegetative growth without genotoxin treatments (Figure 3D and E). This low level phosphorylation was not detected in G1-arrested cells (Supplementary Figure S5C.) and thus could be due to spontaneous DSBs that occur in vegetative growth, and possibly during the premeiotic S phase preceding meiotic DSBs.

Rad51-NTD phosphorylation does not significantly affect the function of Rad51 in repairing DSBs during vegetative growth or meiosis

Next, we examined if Rad51-NTD phosphorylation affects Rad51 function. For comparative purposes, we generated a phosphomimetic mutant (*rad51-3D*) in which all three ser-

ine residues of SQ motifs had been mutated into aspartic acids. Firstly, we found that, as for WT, not only were the phosphorylation variant mutants (*rad51-3A* and *rad51-3D*) resistant to 0.02% MMS during vegetative growth (Figure 2B), but they also generated as many viable spores as WT diploid cells did (Table 1).

Secondly, we found that, like WT Rad51, both Rad51-3A and Rad51-3D exhibited strong Y2H interactions with Hed1, with Rad51-3A presenting a slightly stronger interaction (Figure 1C). Both *dmc1*Δ *rad51-3A* and *dmc1*Δ *rad51-3D* mutants behaved like the *dmc1*Δ mutant in that they failed to generate spores (Table 1), likely due to the inhibitory effect conferred by Hed1 in these strains. Together, these results indicate that $Mec1^{ATR}$/$Tel1^{ATM}$-dependent Rad51-NTD phosphorylation does not seem to affect the Rad51–Hed1 interaction.

We show that phosphorylated Rad51 readily formed foci on chromosomes at the pachytene stage of meiosis (Figure 4B). Rad51 foci detected using antisera targeting native Rad51 and phosphorylated Rad51 did not completely colocalize, implying partial phosphorylation of Rad51 or possible competition for antigen recognition in this assay. Nevertheless, formation of Rad51 foci in the phosphorylation-defective *rad51-3A* mutant was indistinguishable from that of the WT control (Figure 4B–D), despite their delayed appearance on chromosomes (Figure 4E), likely due to low Rad51 protein expression levels (see below). Furthermore, formation of Dmc1 foci was not significantly perturbed in the *rad51-3A* mutant (Figure 4C and D), suggesting that the function of Rad51 in serving as a Dmc1 accessory factor (9) is likely preserved by phosphorylation-defective Rad51-3A.

Both NTD and $Mec1^{ATR}$/$Tel1^{ATM}$-dependent Rad51-NTD phosphorylation are indispensable for meiotic recombination in a *dmc1*Δ *hed1*Δ mutant

Our results reveal that the *dmc1*Δ *hed1*Δ double mutant and the *dmc1*Δ *hed1*Δ *rad51-3D* triple mutant exhibited similar meiotic progression and spore viability to each other (Figure 4A and Table 1), indicating that the Rad51-3D protein is functional for meiotic DSB repair. Moreover, *rad51-3D* behaved like WT *RAD51* in the *dmc1*Δ *hed1*Δ mutant in that delayed meiotic progression and meiosis I non-dysjunction phenotypes (a preponderance of tetrads containing two or zero viable spores) were seen (Figure 4A and Table 1), as reported in a previous study using the *dmc1*Δ *hed1*Δ double mutant (48). Strikingly, both *dmc1*Δ *hed1*Δ *rad51-3A* and *dmc1*Δ *hed1*Δ *rad51-*Δ*N* triple mutants, like the *dmc1*Δ mutant, hardly sporulated (Table 1) and exhibited a strong meiotic progression arrest phenotype at prophase I (Figure 4A). Thus, both Rad51-NTD and Rad51-NTD phosphorylation are essential for Rad51-mediated meiotic recombination in the *dmc1*Δ *hed1*Δ mutant, and the phosphomimetic mutant Rad51-3D can functionally substitute for phosphorylated Rad51 in the same genetic background. This scenario is further supported by the very low spore viability following meiosis of the *dmc1*Δ *hed1*Δ *mec1-kd sml1*Δ strain (Table 1), in which Rad51-NTD phosphorylation is solely dependent on $Tel1^{ATM}$ (Figure 3D, right panel).

To directly determine the impact of Rad51-NTD phosphorylation on Rad51-mediated meiotic recombination, we performed physical analyses to examine if DSB-processing and the yield of interhomolog recombination products, crossovers (COs), at the *HIS4-LEU2* hotspot differed in the *rad51-3A* or *rad51-3D* strains. This hotspot, located on chromosome III, is flanked by XhoI restriction sites (49). Both DSBs and interhomolog COs can be detected by Southern blot analysis of one-dimensional agarose gels using XhoI-digested DNA, and a probe for this region was described previously (42,50) (Supplementary Figure S6A). We found that the WT, *rad51-3A*, *rad51-3D* (Supplementary Figure S6B and C) and *rad51-*Δ*N* strains (Supplementary Figure S6D, second panel from left) all generated similar levels (15–20%) of interhomolog CO products after 12 hours in the sporulation medium (SPM) or by the 24 h time-point. In contrast, in the absence of *DMC1* and *HED1,* these four strains only generated ∼4% interhomolog CO products at the same *HIS4-LEU2* hotspot (Supplementary Figure S6D and E). Five of the mutant strains examined, namely *rad51-*Δ*N*, *dmc1*Δ *hed1*Δ, *dmc1*Δ *hed1*Δ *rad51-3A, dmc1*Δ *hed1*Δ *rad51-3D,* and *dmc1*Δ *hed1*Δ *rad51-*Δ*N*, exhibited less efficiency in DSB repair when compared to WT. The majority of DSBs were repaired and then disappeared in the WT, *rad51-*Δ*N*, *dmc1*Δ *hed1*Δ, and *dmc1*Δ *hed1*Δ *rad51-3D* strains at the 12 h time-point. However, DSBs accumulated in the *dmc1*Δ *hed1*Δ *rad51-*Δ*N* and *dmc1*Δ *hed1*Δ *rad51-3A* triple mutant strains (Supplementary Figure S6F). Accordingly, DDR such as recombination checkpoint was persistently activated only in the *dmc1*Δ *hed1*Δ *rad51-*Δ*N* and *dmc1*Δ *hed1*Δ *rad51-3A* triple mutants, leading to a strong meiotic arrest phenotype in these two mutants (Figure 4A).

Phosphorylation-defective Rad51 sustains scant protein levels during meiosis

Immunoblotting experiments further revealed that the steady-state protein levels of Rad51-3A were lower than those of Rad51 and Rad51-3D in both *DMC1 HED1* and *dmc1*Δ *hed1*Δ meiotic cells (Figure 5A and B). In *DMC1 HED1* meiotic cells, we found the maximum steady-state levels of Rad51-3A (after 7 h in SPM) to be ∼30% those of WT Rad51 (Figure 5B). A comparison of WT Rad51, Rad51-3A and Rad51-3D protein levels in 1-h or 5-h meiotic cultures in the same immunoblot revealed that levels of Rad51-3A stalled and remained less than 30% those of WT Rad51 levels, whereas Rad51-3D was highly abundant and sustained ∼1.4-fold expression relative to WT Rad51 starting from early in meiosis (Figure 5C and D). We conducted immunoblotting analyses on Hop1 and Zip1 to rule out the possibility that the meiotic defects in the *dmc1*Δ *hed1*Δ *rad51-3A* strain were indirectly caused by unscheduled meiotic progression. We did not observe an apparent difference in overall protein level patterns of Hop1 or Zip1 in all six examined strains (Figure 5A and B). Given that phosphorylated Hop1 proteins migrate slower than unphosphorylated Hop1 in SDS polyacrylamide gels (24,25), it is important to note that all three strains in the *dmc1*Δ *hed1*Δ background accumulated more hyperphosphorylated Hop1 even after 12 h in SPM (Figure 5A and B). Similarly, higher levels of phosphorylated Rad51 were also seen in the *dmc1*Δ *hed1*Δ mutants in immunoblots us-

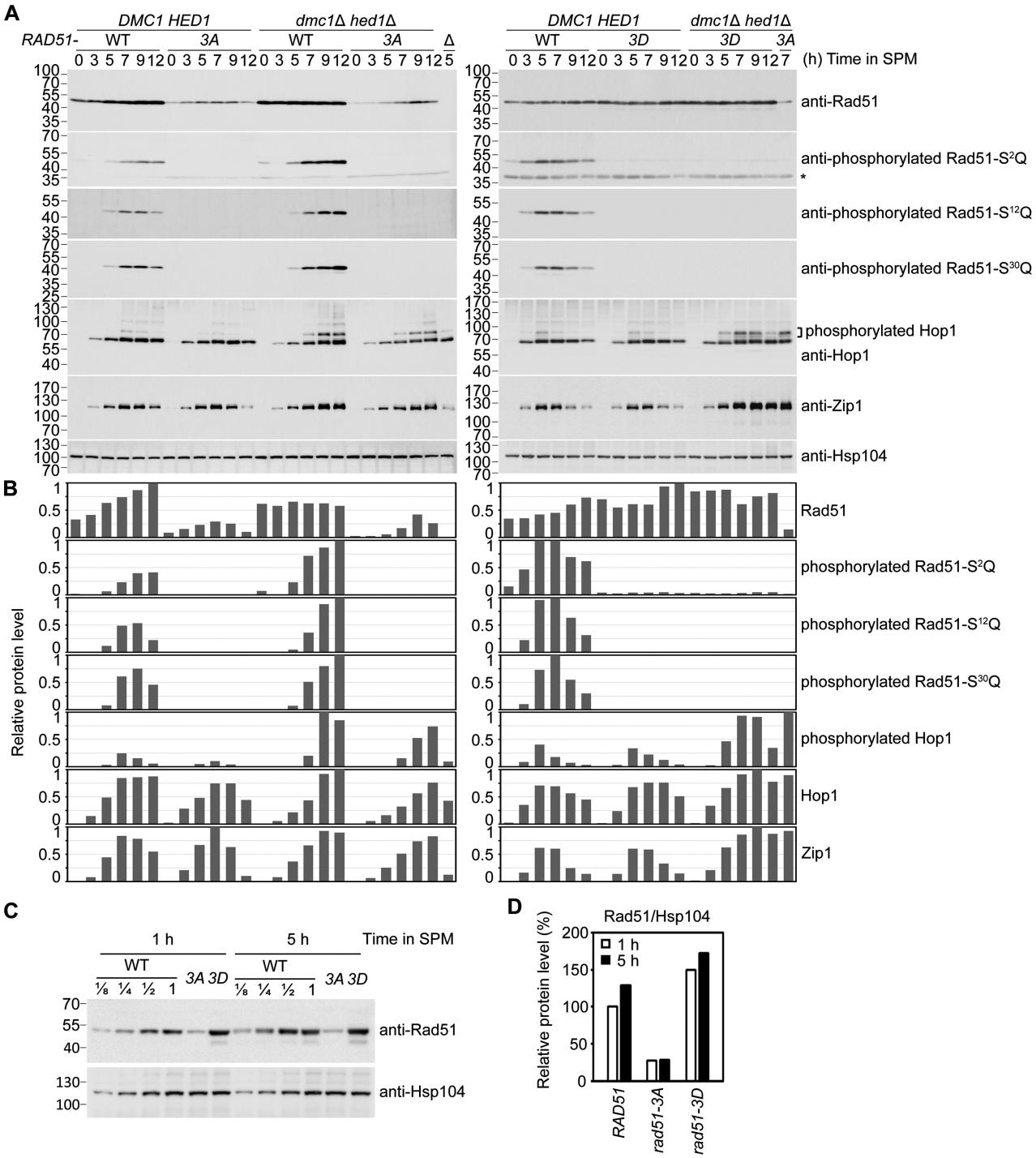

Figure 5. Immunoblotting time-course analyses of WT and the indicated mutant strains were performed as previously described (25,34). (**A**) Total cell lysates were prepared from meiotic cells at indicated sporulation time-points and then visualized by immunoblotting with the corresponding antisera. Antisera against Zip1 and Hop1 were included as references for meiotic progression. Hsp104 was used as a loading control. Size in kilodaltons of standard protein markers is labeled to the left of the blots. The asterisk indicates non-specific bands. (**B**) Quantifications of the protein bands in (A) were normalized to those of Hsp104 at each time-point using ImageJ software and are shown as the relative steady-state levels of indicated proteins. The highest level of immunoblot signal in each blot was used as the standard for comparison. (**C**) Two-fold serial dilutions of WT cell lysates were used to estimate the Rad51 protein levels in *rad51* mutants at 1 h and 5 h in SPM. (**D**) The protein levels of Rad51 variants from non-diluted lysates shown in (C) were quantified and normalized to Hsp104 levels. The Rad51 level of WT at 1 h in SPM was used as the standard.

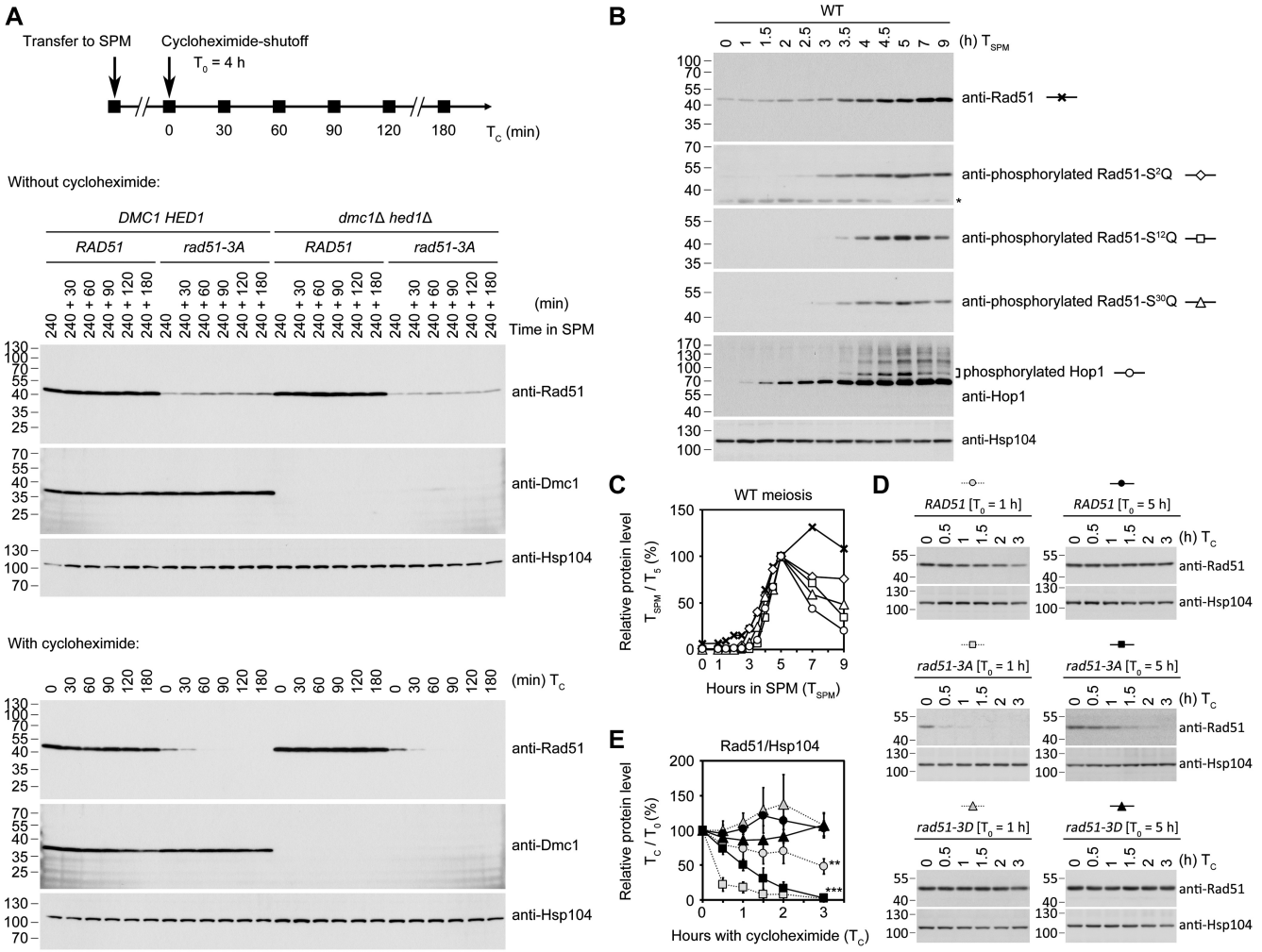

Figure 6. Determination of the half-lives of different Rad51 proteins. **(A)** Cycloheximide-shutoff experiments. Protein synthesis was inhibited by adding 200 μg/ml cycloheximide to the meiotic cultures at the indicated time-points, i.e. 4-h (**A**) or 1-h and 5-h (**D**) after the meiotic cells had been transferred into the sporulation medium. Samples untreated (upper panels) or treated (lower panels) with cycloheximide were taken at 0, 30, 60, 90, 120 and 180 min after the addition of cycloheximide for immunoblotting analysis. (**B**) Immunoblotting time-course analyses of WT meiosis reveal the phosphorylation status of native Rad51 and Hop1. Hsp104 was used as a loading control. (**C**) After normalization to Hsp104 at each time-point in SPM (T_{SPM}), the relative steady-state protein levels in (B) were plotted as compared to those at 5-h (T_5). (**E**) Plot showing relative protein levels in (D). Error bars indicate standard deviation between experiments ($n = 3$). Asterisks indicate values at T_C (hours of cycloheximide treatment) = 3 h that are significantly different from that of WT [$T_0 = 5$ h] at $T_C = 3$ h, with P values calculated using a two-tailed t-test (**P value <0.01 and ***P value <0.001).

ing phospho-specific Rad51-S^{2}Q, Rad51-S^{12}Q, and Rad51-S^{30}Q antisera, respectively (Figure 5A and B). These results could reflect prolonged checkpoint activation by Mec1^{ATR} and Tel1^{ATM} when Dmc1 is absent.

Rad51-NTD phosphorylation results in more stable Rad51 proteins

Next, we carried out cycloheximide-shutoff experiments (41) to compare the protein stability of Rad51, Rad51-3A and Rad51-3D. Protein synthesis was inhibited by adding 200 μg/ml of cycloheximide into meiotic cultures at the 4-h time-point (Figure 6A). Samples were taken at 0, 30, 60, 90, 120 and 180 min after the addition of cycloheximide. Immunoblotting analyses revealed that levels of Rad51 and Dmc1 remained steady in the presence of cycloheximide for up to 180 min. In contrast, within 30 min of adding cycloheximide, levels of Rad51-3A mutant proteins significantly decreased and were barely detectable after 60 min in both the *rad51-3A* and *dmc1*Δ *hed1*Δ *rad51-3A* strains (Figure 6A, lower panels). These results indicate that the half-life ($t_{1/2}$) of Rad51-3A is ≤30 min, whereas the $t_{1/2}$ of Rad51 and Dmc1 are ≥180 min.

In our time-course experiments on WT strains with 30 min intervals between sample collection, we found that native Rad51 protein levels gradually increased along with progression of meiosis, accompanied by gradual phosphorylation of the three SQ motifs (Figure 6B and C). We speculate that during early meiosis (i.e. at the 1-h meiotic time-point), unphosphorylated native Rad51 (but not Rad51-3D) could be labile to a similar extent as Rad51-3A at the 4-h time-point ($t_{1/2} \leq 30$ min) and would be stabilized upon phosphorylation of Rad51-NTD when entering later meiosis. We carried out cycloheximide-shutoff assays using

aliquots of the same culture shown in Figure 6B at different time-points and compared the stability of WT Rad51, Rad51-3A and Rad51-3D from 1-h and 5-h meiotic cultures. Our results show that native Rad51 from the 5-h meiotic culture is indeed more stable ($t_{1/2} \geq 180$ min) than that from the 1-h meiotic culture ($t_{1/2} \approx 180$ min) (Figure 6D and E). We further demonstrate that the phosphomimetic mutant (Rad51-3D) in the 1-h or 5-h meiotic culture is as stable as native Rad51 from 5-h meiotic culture ($t_{1/2} \geq 180$ min) (Figure 6D and E), suggesting that the negatively-charged NTD is sufficient to stabilize Rad51 during meiosis.

Thus, phosphorylation of Rad51-NTD plays an important role in enhancing protein stability of Rad51. When Dmc1 was present in the *rad51-3A* strain, low steady-state levels of Rad51-3A apparently were sufficient to facilitate Dmc1 in mediating meiotic recombination, which is consistent with our cytological observations (Figure 4C and D). In contrast, when Rad51 is the only 'active' recombinase in the meiotic cells (i.e. in the *dmc1*Δ *hed1*Δ strain), phosphorylation of Rad51-NTD is essential to ensure higher steady-state levels of Rad51 in order to repair the DSBs induced by Spo11. Moreover, phosphorylated Rad51 can be functionally substituted by Rad51-3D.

Rescue of the sporulation defects in *dmc1*Δ *hed1*Δ *rad51-3A* and *dmc1*Δ *hed1*Δ *rad51-*Δ*N* triple mutants by overexpressing WT Rad51 or Rad51-3A

Insufficient expression of Rad51 proteins may explain the sporulation defects of *dmc1*Δ *hed1*Δ *rad51-3A* and the lower spore viability phenotype of *rad51-*Δ*N* mutants. To test this hypothesis, we introduced high-copy number vectors expressing WT Rad51, Rad51-3A or Rad51-ΔN into four different diploid mutants that exhibited different levels of meiotic deficiencies, namely *rad51*Δ (no viable spores), *rad51-*Δ*N* (∼50% spore viability), *dmc1*Δ *hed1*Δ *rad51-3A* and *dmc1*Δ *hed1*Δ *rad51-*Δ*N* (MI arrest). Relative to yeast mutants transformed with the mock control vector, overexpression of WT Rad51 could rescue the meiotic defects (low spore viability or the sporulation deficiency phenotype) of all four of these diploid mutants (Table 2). Although overexpression of Rad51-3A failed to rescue the meiotic prophase arrest phenotype of *dmc1*Δ, in which Hed1 was present, overexpression of Rad51-3A not only fully restored the spore viability of *rad51*Δ, but also successfully rescued the sporulation defect of *dmc1*Δ *hed1*Δ *rad51-3A* and restored its spore viability to a level comparable to that of the *dmc1*Δ *hed1*Δ strain harboring overexpression vectors for either WT Rad51 or mock (Table 2). In addition, overexpression of Rad51-ΔN partially rescued the low spore viability of *rad51*Δ but not *rad51-*Δ*N*, indicating that Rad51-ΔN is capable of supporting meiotic recombination but is less efficient than WT Rad51. Overexpression of Rad51-ΔN was also unable to rescue the sporulation defects of the *dmc1*Δ *hed1*Δ *rad51-*Δ*N* strain (Table 2), suggesting that despite being expressed from a high-copy vector with its own promoter, Rad51-ΔN overexpression only exhibited mild or negligible effects when meiotic cells suffered from insufficient levels of Rad51 proteins.

We also performed meiotic time-course immunoblotting experiments to confirm that introducing the high-copy number Rad51-3A expression vector indeed resulted in higher Rad51-3A protein levels in the *dmc1*Δ *hed1*Δ *rad51-3A* strain relative to introduction of mock vectors (Supplementary Figure S7). In contrast, transformation of the high-copy number Rad51-ΔN overexpression vector barely increased Rad51-ΔN protein levels in the *rad51-*Δ*N* (Supplementary Figure S3A) or *dmc1*Δ *hed1*Δ *rad51-*Δ*N* (Supplementary Figure S3B) strains compared to mock vector.

These results support our hypothesis that low steady-state levels of Rad51-3A and Rad51-ΔN proteins are the main cause of meiotic defects in the mutant strains (Tables 1 and 2).

Table 2. Spore viability of yeast strains with overexpression plasmids

Strain	Overexpression plasmid[a]	Spore viability
WT	*2μ-bsd-RAD51*	100% ($n = 144$)
*rad51*Δ	*2μ-bsd-RAD51*	98% ($n = 288$)
*rad51-*Δ*N*	*2μ-bsd-RAD51*	80% ($n = 144$)
*dmc1*Δ *hed1*Δ	*2μ-bsd-RAD51*	83% ($n = 216$)
*dmc1*Δ *hed1*Δ *rad51-3A*	*2μ-bsd-RAD51*	85% ($n = 216$)
*dmc1*Δ *hed1*Δ *rad51-*Δ*N*	*2μ-bsd-RAD51*	81% ($n = 144$)
WT	*2μ-bsd-rad51-3A*	47% ($n = 216$)
*rad51*Δ	*2μ-bsd-rad51-3A*	97% ($n = 216$)
*dmc1*Δ	*2μ-bsd-rad51-3A*	No spore formation
*dmc1*Δ *hed1*Δ	*2μ-bsd-rad51-3A*	86% ($n = 216$)
*dmc1*Δ *hed1*Δ *rad51-3A*	*2μ-bsd-rad51-3A*	79% ($n = 216$)
WT	*2μ-bsd-rad51-*Δ*N*	97% ($n = 144$)
*rad51*Δ	*2μ-bsd-rad51-*Δ*N*	63% ($n = 144$)
*rad51-*Δ*N*	*2μ-bsd-rad51-*Δ*N*	54% ($n = 144$)
*dmc1*Δ *hed1*Δ *rad51-*Δ*N*	*2μ-bsd-rad51-*Δ*N*	No spore formation
*rad51*Δ	mock	0% ($n = 144$)
*rad51-*Δ*N*	mock	38% ($n = 144$)
*dmc1*Δ *hed1*Δ	mock	88% ($n = 216$)
*dmc1*Δ *hed1*Δ *rad51-3A*	mock	No spore formation
*dmc1*Δ *hed1*Δ *rad51-*Δ*N*	mock	No spore formation

[a]Yeast diploid cells were respectively transformed with the indicated *2μ* overexpression vector. Resistance to blasticidin is conferred by the product of the blasticidin S deaminase (*bsd*) gene from *Aspergillus terreus*. The *RAD51*, *rad51-3A* and *rad51-*Δ*N* genes were expressed under the native *RAD51* promoter.

Unphosphorylated Rad51 proteins are degraded via the proteasomal pathway

The 26S proteasome has been shown to be required for HDRR in *S. cerevisiae* (51). Next, we used the proteasome inhibitor MG132 to determine if WT Rad51 and Rad51-3A are degraded by proteasomes during the DNA damage response. To facilitate uptake of MG132, the strains were deleted of *PDR5* to reduce efflux pump activity. After a 30-min treatment of MMS, Rad51-3A disappeared more rapidly than WT Rad51 under cycloheximide treatment (Figure 7A–C). In contrast, simultaneous addition of MG132 and cycloheximide postponed the degradation of Rad51-3A, indicating that Rad51-NTD phosphorylation stabilizes Rad51 protein by preventing proteasomal degradation during the DNA damage response.

To determine phosphorylation of which SQ motif in Rad51-NTD is the most important for its stability, we carried out cycloheximide-shutoff experiments to determine the relative protein stabilities of Rad51-S2A, Rad51-S12A and Rad51-S30A (Figure 7D). Our results show that all

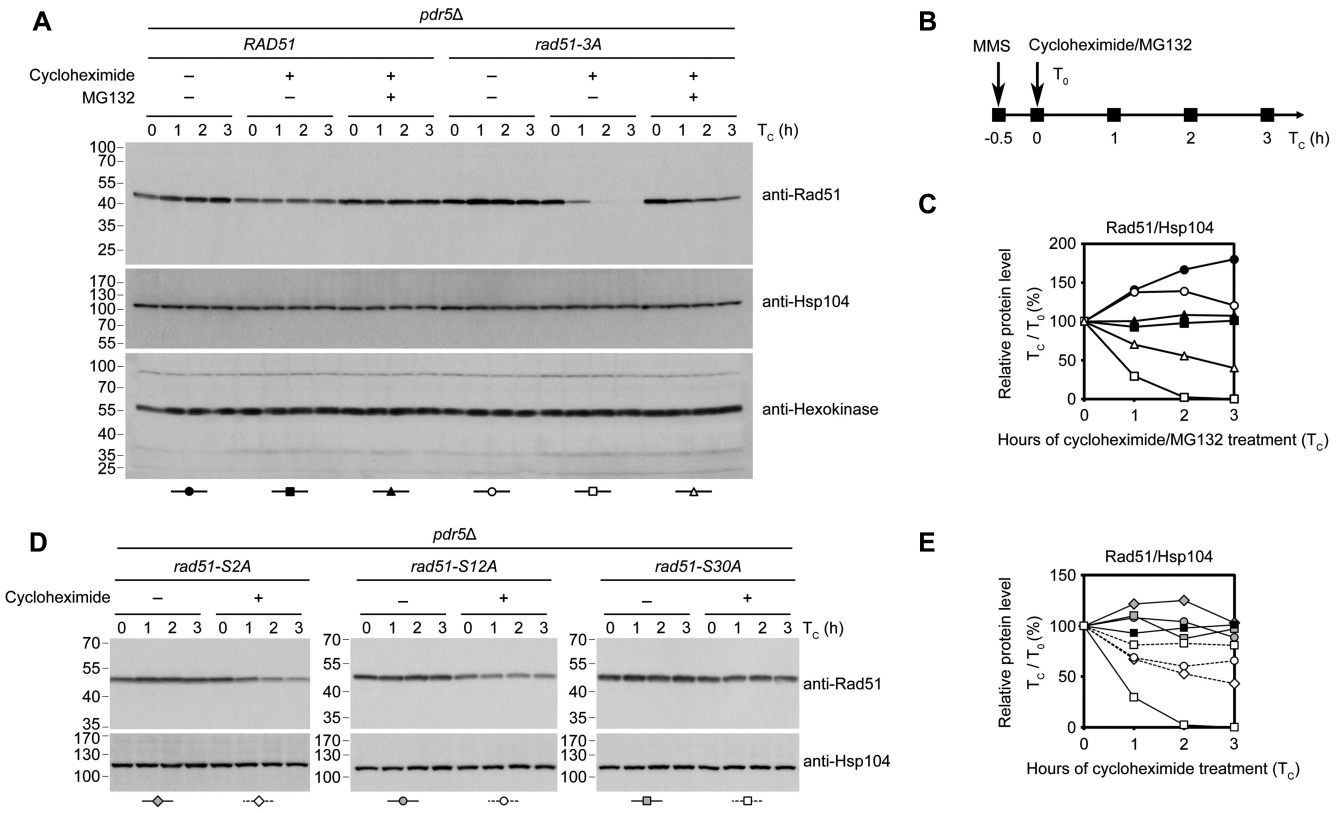

Figure 7. Rad51-3A is degraded by the 26S proteasome. Exponential cultures of indicated strains were treated with MMS (0.02%) 30 min prior to the addition of cycloheximide (200 μg/ml) and/or MG132 (25 μM). Protein samples were harvested at indicated time-points and immunoblotting was performed as described in Figure 6. To decrease MG132 efflux, we deleted the *PDR5* gene, which encodes an ABC transporter. The protein levels of another vegetative house-keeping protein, hexokinase, were analyzed by immunoblotting using anti-hexokinase antibodies and are shown as the loading control in (A). Quantification of immunoblotting results in (**A**) and (**D**) are plotted in (**C**) and (**E**), respectively, in which total Rad51 protein levels normalized to Hsp104 levels at that time-point are plotted. Quantification results of samples of WT and *rad51-3A* with cycloheximide from (C) were included in (E) for comparison.

three of these Rad51 protein variants were less stable than WT Rad51, but they were much more stable than Rad51-3A, with the least stable mutant protein Rad51-S2A exhibiting a half-life of ∼3 h (Figure 7E). Thus, phosphorylation of each of the SQ motifs in Rad51-NTD collaboratively contributes to Rad51 protein stabilization.

Rad51-NTD can act autonomously to promote expression of an exogenous protein, β-galactosidase

Our results indicate that Rad51-NTD contains an SCD and it possesses a novel function in promoting high steady-state levels of Rad51 proteins during DDR of vegetative growth as well as in meiosis. Remarkably, this function could be independent of $Mec1^{ATR}$/$Tel1^{ATM}$-dependent Rad51-NTD phosphorylation. To further characterize its biochemical properties, we modified an *S. cerevisiae* pYC2/CT/P_{GAL1}-LacZ-V5-His_6 low-copy number expression vector (Invitrogen, USA) into P_{RAD51}-LacZ-NLS-V5-His_6 by replacing the *GAL1* promoter with the promoter of the wild-type *RAD51* gene (P_{RAD51}) and inserting an SV40 nuclear localization signal (NLS) peptide preceding a V5 epitope tag and a hexahistidine affinity tag. Next, we constructed three corresponding mutant vectors: P_{RAD51}-NTD^{WT}-LacZ-NLS-V5-His_6, P_{RAD51}-NTD^{3A}-LacZ-NLS-V5-His_6 and P_{RAD51}-NTD^{3D}-LacZ-NLS-V5-His_6. All four of these vectors were transformed into an SK1 yeast strain. The transformants were vegetatively propagated to reach logarithmic phase and then harvested for denatured lysate preparation. Immunoblotting analyses using the antisera against phosphorylated Rad51-$S^{12}Q$ indicated that $Tel1^{ATM}$ and $Mec1^{ATR}$ can phosphorylate NTD^{WT}-LacZ-NLS-V5-His_6, but not NTD^{3A}-LacZ-NLS-V5-His_6 or NTD^{3D}-LacZ-NLS-V5-His_6 (Figure 8A). All three of these fusion proteins could be recognized in immunoblottings by the anti-Rad51 antiserum, and the order of steady-state protein levels was NTD^{WT}-LacZ-NLS-V5-His_6 ≈ NTD^{3D}-LacZ-NLS-V5-His_6 > NTD^{3A}-LacZ-NLS-V5-His_6 (Figure 8A), all of which showed apparently higher protein levels than for LacZ-NLS-V5-His_6 (Figure 8B). A similar hierarchy of protein levels was also observed when Rad51 variants were fused to exogenous proteins such as LexA and were expressed from high-copy number vectors (Supplementary Figure S2B). Thus, NTD^{WT}, NTD^{3A}, and NTD^{3D} all possess the capability to enhance expression of their fusion partner, LacZ-NLS-V5-His_6. Notably, NTD^{3A}-LacZ-NLS-V5-His_6 was more labile than NTD^{WT}-LacZ-NLS-V5-His_6 and NTD^{3D}-LacZ-NLS-V5-

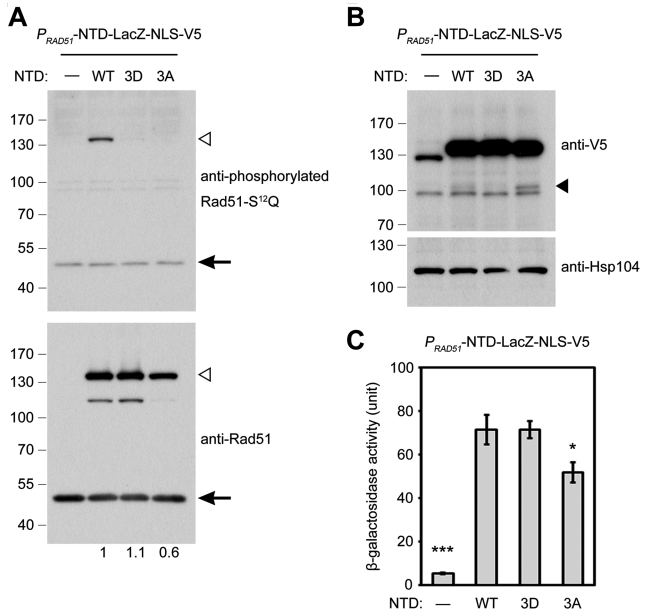

Figure 8. Rad51-NTD is a tunable 'nanny' peptide. The wild-type SK1 haploid strain was transformed with an indicated yeast expression vector, i.e. P_{RAD51}-LacZ-NLS-V5 (mock), P_{RAD51}-NTD^{WT}-LacZ-NLS-V5, P_{RAD51}-NTD^{3A}-LacZ-NLS-V5 or P_{RAD51}-NTD^{3D}-LacZ-NLS-V5. (**A, B**) Immunoblotting. Total cell lysates were prepared from mitotic cells undergoing exponential growth for visualization by immunoblotting with the corresponding antisera and quantitative yeast LacZ assays in (C). (**A**) NTD-LacZ-NLS-V5 fusion proteins (~128 kDa) are indicated by white arrowheads. Endogenous Rad51 (~43 kDa) is indicated by black arrows. Numbers below the anti-Rad51 immunoblot indicate fold-changes of NTD-LacZ-NLS-V5 fusion protein levels normalized to endogenous Rad51 protein levels in the same blot. (**B**) Immunoblotting using anti-V5 antiserum. Presumptively degraded products are indicated by black arrowheads. Hsp104 was used as a loading control. (**C**) Quantitative yeast LacZ assays were performed as described previously (41). Error bars indicate standard deviation between experiments. ($n = 3$). Asterisks indicate significant differences when compared to NTD^{WT}, with P values calculated using a two-tailed t-test (*P value < 0.05 and ***P value < 0.001).

His_6, given that there were more degraded NTD^{3A}-LacZ-NLS-V5-His_6 products in the immunoblot (Figure 8B, indicated by the black arrowhead). We also determined the β-galactosidase activities of these four fusion proteins (see 'Materials and Methods' section). The hierarchy (and normalized relative activity level) was NTD^{3D}-LacZ-NLS-V5-His_6 (13.2-fold) ≈ NTD^{WT}-LacZ-NLS-V5-His_6 (13.2-fold) > NTD^{3A}-LacZ-NLS-V5-His_6 (9.6-fold) >> LacZ-NLS-V5-His_6 (Figure 8C). The observation that NTD^{WT} and NTD^{3D} exhibited almost the same ability to facilitate protein levels of their fusion partners may imply that most (if not all) of the NTD^{WT}-LacZ-NLS-V5-His_6 fusion proteins are phosphorylated dependently on Tel1^{ATM} and Mec1^{ATR}.

Together with our results showing that the order of steady-state protein levels of Rad51 variants is Rad51 > Rad51-3A >> Rad51-ΔN in both vegetative and meiotic cells, we suggest that our findings reveal that Rad51-NTD has at least two independent functions for maintaining high steady-state levels of Rad51 *in vivo*. First, Rad51-NTD acts autonomously to promote expression (and/or folding) of its fusion partner. Second, Rad51-NTD is also an SCD that is phosphorylated by Tel1^{ATM} and Mec1^{ATR} to enhance Rad51 protein stability via antagonizing proteasomal degradation.

Phosphorylation on serine residues of SQ motifs but not other serines or threonines in Rad51-NTD is critical for maintaining steady-state protein levels of Rad51

We propose that Tel1^{ATM}- and Mec1^{ATR}-dependent phosphorylation of Rad51-NTD at S^{2}Q, S^{12}Q and S^{30}Q antagonizes the proteasomal degradation of Rad51. To decipher if other serines and threonines in the Rad51-NTD are also phosphorylated to promote Rad51 stability, we generated an additional *rad51* mutant (*rad51-8A*) in which the three serines of the SQ motifs were retained but all the other serines and threonines in the Rad51-NTD were mutated into alanines (Figure 9A). A further *rad51* mutant (*rad51-11A*) in which all serines and threonines of Rad51-NTD were substituted to alanines was also generated for comparison. Growth of these two new mutant strains on YPD plates containing MMS was indistinguishable from that of WT or the *rad51-3A* mutant strain and, unlike the *rad51-ΔN* strain, they did not show apparent hypersensitivity when grown on YPD plates with 0.02% MMS (Figure 9B, upper panel). Immunoblotting experiments to analyze Rad51 protein levels upon MMS treatment revealed that there was a comparable reduction of the steady-state protein levels of Rad51-11A (~45% lower) to that of Rad51-3A (~30% lower), whereas the *rad51-8A* mutant strain maintained similar levels of Rad51 protein to WT (Figure 9C). Thus, phosphorylation of the three SQ motifs in Rad51-NTD is critical for antagonizing the proteasomal degradation of Rad51, whereas phosphorylation of the other serines or threonines in Rad51-NTD is irrelevant to that function.

Comparative analysis of Rad51-NTD phosphorylation and Rad51-S^{192}Q phosphorylation

It was reported previously that Rad51-S^{192}Q, the fourth SQ motif in Rad51, might be phosphorylated by Mec1^{ATR} (44). Those authors generated a phospho-specific Rad51-S^{192}Q antibody to validate S^{192}Q phosphorylation on bacterially-purified Rad51 proteins subjected to DNA-PK (DNA-dependent protein kinase)-catalyzed phosphorylation *in vitro*, given that DNA-PK is a phosphatidylinositol 3-kinase-related protein kinase enzyme with a similar SQ target consensus sequence to that of Mec1^{ATR} and Tel1^{ATM} (52). Phosphorylation of S^{192}Q on purified yeast-expressed epitope-tagged Rad51 proteins (i.e. Rad51-TAP and Rad51-Myc) were also analyzed in that study using that antibody (44). The authors proposed that S^{192}Q phosphorylation could influence homologous recombination by mimicking the ATP- or ADP-bound form of Rad51, which can form a catalytically inactive multimer (44). Since both the phosphorylation-defective mutation (*rad51-S192A*) and the phosphomimetic mutation (*rad51-S192E*) impaired Rad51 function *in vivo* (44), the exact role of Rad51-S^{192}Q phosphorylation had remained unclear.

We were unable to generate antisera specific for phosphorylated Rad51-S^{192}Q protein (see 'Materials and Methods' section) to compare the biological function(s) of Rad51-NTD phosphorylation and Rad51-S^{192}Q phosphorylation.

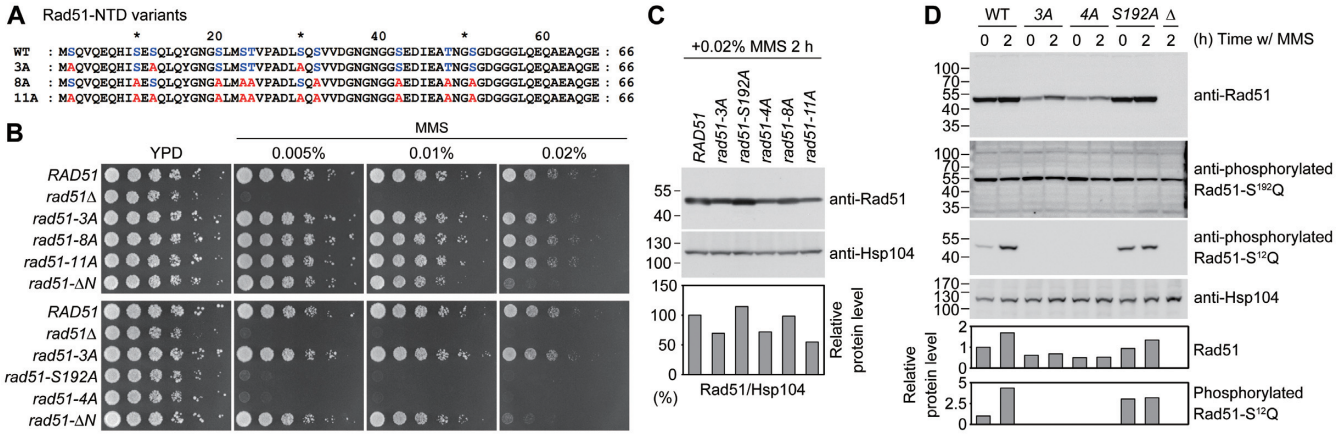

Figure 9. Characterization of the functions of other probable phosphorylation targets in Rad51-NTD and the fourth SQ motif. (**A**) Protein sequence alignments showing Rad51-NTD variants with serines and threonines (blue) replaced by alanines (red), as indicated. (**B**) Spot assay showing five-fold serial dilutions of haploid yeast strains, performed as described in Figure 2. (**C, D**) Total cell lysates were prepared from mitotic cells under MMS (0.02%) treatment and analyzed using immunoblots, as described in Figure 3. Protein levels were quantified and normalized to Hsp104 levels. Protein levels from WT lysates of MMS-treated cultures were a standard for comparison in (C). WT lysates without MMS treatment were used as a standard for comparison in (D).

Instead, we generated two additional mutants, i.e. *rad51-S192A* and *rad51-4A*. In *rad51-4A*, all four SQ motifs (S^2Q, $S^{12}Q$, $S^{30}Q$, and $S^{192}Q$, highlighted in red in Figure 1B) of endogenous Rad51 were mutated to AQ. We first confirmed that *rad51-S192A* and *rad51-4A*, like *rad51*Δ (but not WT or *rad51-3A*), exhibited hypersensitivity to 0.005% MMS during vegetative growth (Figure 9B, lower panel). Consistent with the findings of the previous report (44), our *rad51-S192A* strain was indeed defective in repairing DSBs. We obtained the phospho-specific Rad51-$S^{192}Q$ antibody (44) as a kind gift from Stephen Jackson (University of Cambridge). However, we could not reproduce the specificity in immunoblotting experiments when examining our five yeast strains, namely *RAD51*, *rad51-3A*, *rad51-4A*, *rad51-S192A* and *rad51*Δ (Figure 9D), perhaps due to differences in strain background or experimental procedures. Next, we showed by immunoblotting with anti-Rad51 antisera that the state-steady protein levels of Rad51-S192A was similar to those of WT Rad51, but higher than those of Rad51-3A or Rad51-4A, during DDR in vegetative growth (Figure 9D). Using antisera specific for phosphorylated Rad51-$S^{12}Q$, we also found that WT Rad51 and Rad51-S192A, but not Rad51-3A or Rad51-4A, underwent MMS-induced $S^{12}Q$ hyperphosphorylation (Figure 9D). Intriguingly, the *rad51-S192A* mutant showed a higher level of $S^{12}Q$ phosphorylation without MMS treatment, suggesting that DDR might be induced in this mutant even without exposure to DNA damaging agents.

We propose that phosphorylation of all three SQ motifs in Rad51-NTD plays an important role in promoting Rad51 protein stability and that this function can be recapitulated by phosphomimetic mutations. In contrast, the SQ motif ($S^{192}Q$) adjacent to the ATPase domain is required for the catalytic activity of Rad51, but is not related to Rad51 protein abundance control. Since the phosphomimetic mutation *rad51-S192E* has been reported defective in Rad51 recombinase activity but not in protein folding and/or multimerization (44), further investigations are needed to decipher why negative charges on these four SQ motifs of Rad51 by phosphomimetic mutations render such distinct impacts.

DISCUSSION

The *RAD51* gene of *S. cerevisiae* was first cloned in 1992 (6). Many investigations have since been conducted to establish its molecular functions in various biological processes (1,2). In this report, we show that three SQ motifs (S^2Q, $S^{12}Q$ and $S^{30}Q$) in Rad51-NTD are phosphorylated in a $Tel1^{ATM}$- and $Mec1^{ATR}$-dependent manner during both vegetative growth and meiosis. Thus, the function of Rad51 is directly regulated by the DNA damage checkpoint in *S. cerevisiae*. It was proposed previously that *S. cerevisiae* Rad51 was transiently phosphorylated at the $S^{192}Q$ motif primarily mediated by $Mec1^{ATR}$ (44) given that the phosphomimetic mutation of *rad51-S192E* could not functionally substitute this postulated phosphorylation. Thus, the biological functions involving the putative negatively charged $S^{192}Q$ motif remains obscure.

Here, we demonstrate that the function of $Mec1^{ATR}$/$Tel1^{ATM}$–dependent Rad51-NTD phosphorylation is to enhance Rad51 protein stability by antagonizing the proteasomal pathway. The half-life ($t_{1/2}$) of the phosphorylation-defective Rad51-3A mutant is ≤30 min, whereas $t_{1/2}$ of phosphorylated WT Rad51 or phosphomimemtic Rad51-3D is ≥180 min (Figure 6E). Based on our cycloheximide-shutoff experiments (Figure 6), which show that WT Rad51 at 5-h meiosis is as stable as Rad51-3D, we infer that most (if not all) of the Rad51 protein is likely phosphorylated in response to MMS-induced or meiotic DSBs *in vivo*. Basal levels of Rad51-NTD phosphorylation also occur in the absence of exogenous DNA lesions or meiotic DSBs and are likely related to spontaneous damages in S phase (Supplementary Figure S5). This unique property also readily explains why Rad51 phosphorylation has distinct

impacts on Rad51-mediated DNA repair during vegetative growth and meiosis. Previous studies in *S. cerevisiae* have reported mitotic S phase durations of 20–30 min (53,54). During synchronous SK1 meiosis, S phase lasts 65–80 min (55,56), and Spo11-induced DSBs take place at 1.5–3.5 h (57). Subsequently, the chromosomal foci of two RecA-like recombinases were shown to appear and disappear within a single peak (2.5–5 h), with maximum abundance at 3 h (43). Accordingly, Rad51-NTD phosphorylation is dispensable for DNA damage repair during vegetative growth. In contrast, phosphorylation-defective mutant Rad51-3A proteins in the *dmc1*Δ *hed1*Δ mutant are not stable enough to support such a long period of Spo11-induced DSB repair during meiosis (Table 1). The Rad51-NTD phosphorylation pathway we describe here supports the notion that $Mec1^{ATR}$ alone can perform most of the functions of $Tel1^{ATM}$ and $Mec1^{ATR}$ together in *S. cerevisiae* (58,59), and that $Mec1^{ATR}$ has an essential function in regulating protein homeostasis (38,39). It will be important to further examine if genetic interaction partners of $Mec1^{ATR}$ that are involved in protein homeostasis (38,39) are also responsible for regulating Rad51 homeostasis, thereby affecting the outcomes of Rad51- and Dmc1-mediated meiotic recombination.

The second important finding of this study is that Rad51-NTD possesses an autonomous 'nanny' function and promotes expression and/or folding of its C-terminal fusion partners (e.g. Rad51-ΔN and LacZ). Although the steady-state levels of Rad51-ΔN are ≤3% those of wild-type Rad51 in both vegetative and meiotic cells, the *rad51-ΔN* allele only affected DSB repair when vegetative cells were exposed to high concentrations of MMS or in the *dmc1*Δ *hed1*Δ meiotic cells. Moreover, the *rad51-ΔN* diploid cells could still generate ∼50% viable spores (Table 1). We suggest that in order to tolerate scenarios with excessive DSBs, Rad51-NTD evolved specifically to maintain superfluous amounts of Rad51 *in vivo*. For example, it takes a long time (≥3 h) to repair genome-wide DSBs induced by Spo11 in *S. cerevisiae* meiosis, so high steady-state levels of Rad51 are required over a long time-period.

Our results have also revealed that the *sml1*Δ allele is a suppressor of deficiencies elicited by *rad51-ΔN* in terms of the less growth phenotype induced by DNA lesions during vegetative growth (Figure 2A) and the low spore viability phenotype in meiosis (Table 1). Therefore, with regard to *sml1*Δ repression, *rad51-ΔN* is phenotypically similar to *mec1-kd*. Further investigations will reveal whether and how the absence of Sml1 proteins in *sml1*Δ (or an increase of dNTP abundance) ameliorates the deleterious effects caused by *rad51-ΔN*. Since the steady-state levels of Rad51-ΔN in *rad51-ΔN* cells are not significantly different from those in *rad51-ΔN sml1*Δ cells during vegetative growth (Figure 3B), we reason that Rad51 might be an abundant target of $Mec1^{ATR}$ and $Tel1^{ATM}$ in *S. cerevisiae* in the sense that deficiency of either Rad51-NTD or Mec1 would result in a similar outcome in terms of suppression by *sml1*Δ. Along with this hypothesis, it was recently reported (60) (*Saccharomyces* Genome Database: https://www.yeastgenome.org) that the median abundance of Rad51 (6070 ± 2766 molecules/cell) in vegetative cells is higher than those of other known $Mec1^{ATR}$ and $Tel1^{ATM}$ target proteins, e.g. Rad9 (1279 ± 701 molecules/cell), Rad53 (1533 ± 520 molecules/cell) and Sae2 (1084 ± 93 molecules/cell). Whether these proteins involved in the DDR network are subjected to the same degree of protein quality control by $Mec1^{ATR}$ and $Tel1^{ATM}$ as Rad51 remains to be characterized.

In conclusion, due to the presence of the Rad51-NTD, *S. cerevisiae* can ensure sufficient levels of Rad51 to deal with extreme physiological conditions such as excessive DNA damage or long periods of DNA repair. This intriguing characteristic might explain two unique properties found in this important model organism: (1) HDRR is the dominant repair mode for DSBs in *S. cerevisiae*; and (2) inhibition of Rad51 by Hed1 ensures Dmc1-mediated HDRR outperforms Rad51-mediated HDRR during meiosis. This latter function is particularly critical for hybrid meiosis of polymorphic homologous chromosomes (10), because Dmc1 is superior to Rad51 in tolerating mismatched sequences during their strand exchange reaction (11,12). Accordingly, our results also explain why both Rad51-NTD and Hed1 (a meiosis-specific inhibitor of Rad51) are specific to the genus *Saccharomyces*. Since the duration of the meiotic program is, in general, longer than that of mitotic progression (61), it would be intriguing to investigate if Rad51 proteins in other sexual eukaryotes are regulated differentially during mitosis and meiosis and if novel meiosis-specific accessory factor(s) have evolved to promote or retain high steady-state Rad51 protein levels upon encountering robust DNA damage.

Inspired by the findings of this study, we recently showed that the SCDs of several other yeast DDR proteins [e.g. Rad53-SCD1 (amino acid residues 1–29), Hop1-SCD (amino acid residues 258–324) and Sml1-SCD (amino acid residues 1–50, personal communications with Rita Cha, Bangor University)] possess autonomous and exchangeable activities to enhance high-level protein expression when they are artificially designed as NH_2-terminal fusion tags of LacZ, GFP, etc. We also discovered an interesting correlation between relative LacZ activities and the overall S/T/Q percentages in the total amino acid content of these intrinsically disordered regions (IDRs) given that low sequence complexity and high S/T/Q content are characteristic features of IDRs in proteins (62). To attain optimal LacZ activity of >8-fold, overall S/T/Q content of IDRs should range from 30% to 40% (unpublished results). Intriguingly, the enrichment of S/T-Q motifs in SCDs means that they exhibit low sequence complexity (19). Taken together, our results have not only revealed that SCDs can promote protein expression but also supported that $Mec1^{ATR}$ could regulate protein homeostasis.

SUPPLEMENTARY DATA

Supplementary Data are available at NAR Online.

ACKNOWLEDGEMENTS

We thank Douglas Bishop (University of Chicago), Stephen Jackson (University of Cambridge) and Chung Wang (Academia Sinica) for providing antisera used in this study, Valentin Börner (Cleveland State University) for technical advice for physical analysis experiments, Rita Cha (Bangor University) for discussion of her unpublished results on

Sml1 in regulating protein homeostasis, and John O′Brien for English editing.
Author contributions: T.T.W. and C.N.C. performed the experiments and analyzed the data. T.T.W. and T.F.W. conceived and designed the experiments and wrote the paper. M.H. and A.S. provided antisera and technical advice for cytological experiments. All of the authors read and approved the manuscript.

FUNDING

Academia Sinica, Taiwan [AS-105-TP-B07, AS108-TP-B07 to T.F.W.]; Ministry of Science and Technology, Taiwan, Republic of China [MOST163-2311-B-001-016-MY3 to T.F.W.]; T.T.W. was supported by postdoctoral fellowships from Academia Sinica and MOST. Funding for open access charges: Academia Sinica [AS108-TP-B07 to T.F.W.].
Conflict of interest statement. None declared.

REFERENCES

1. Daley,J.M., Gaines,W.A., Kwon,Y. and Sung,P. (2014) Regulation of DNA pairing in homologous recombination. *Cold Spring Harb. Perspect. Biol.*, **6**, a017954.
2. Kowalczykowski,S.C. (2015) An overview of the molecular mechanisms of recombinational DNA repair. *Cold Spring Harb. Perspect. Biol.*, **7**, a016410.
3. Zickler,D. and Kleckner,N. (1999) Meiotic chromosomes: integrating structure and function. *Annu. Rev. Genet.*, **33**, 603–754.
4. Hunter,N. (2015) Meiotic recombination: the essence of heredity. *Cold Spring Harb. Perspect. Biol.*, **7**, a016618.
5. Brown,M.S. and Bishop,D.K. (2014) DNA strand exchange and RecA homologs in meiosis. *Cold Spring Harb. Perspect. Biol.*, **7**, a016659.
6. Shinohara,A., Ogawa,H. and Ogawa,T. (1992) Rad51 protein involved in repair and recombination in *S. cerevisiae* is a RecA-like protein. *Cell*, **69**, 457–470.
7. Bishop,D.K., Park,D., Xu,L. and Kleckner,N. (1992) *DMC1*: a meiosis-specific yeast homolog of *E. coli recA* required for recombination, synaptonemal complex formation, and cell cycle progression. *Cell*, **69**, 439–456.
8. Tsubouchi,H. and Roeder,G.S. (2006) Budding yeast Hed1 down-regulates the mitotic recombination machinery when meiotic recombination is impaired. *Genes Dev.*, **20**, 1766–1775.
9. Cloud,V., Chan,Y.L., Grubb,J., Budke,B. and Bishop,D.K. (2012) Rad51 is an accessory factor for Dmc1-mediated joint molecule formation during meiosis. *Science*, **337**, 1222–1225.
10. Callender,T.L., Laureau,R., Wan,L., Chen,X., Sandhu,R., Laljee,S., Zhou,S., Suhandynata,R.T., Prugar,E., Gaines,W.A. *et al.* (2016) Mek1 down regulates Rad51 activity during yeast meiosis by phosphorylation of Hed1. *PLoS Genet.*, **12**, e1006226.
11. Lee,J.Y., Terakawa,T., Qi,Z., Steinfeld,J.B., Redding,S., Kwon,Y., Gaines,W.A., Zhao,W., Sung,P. and Greene,E.C. (2015) DNA RECOMBINATION. Base triplet stepping by the Rad51/RecA family of recombinases. *Science*, **349**, 977–981.
12. Qi,Z., Redding,S., Lee,J.Y., Gibb,B., Kwon,Y., Niu,H., Gaines,W.A., Sung,P. and Greene,E.C. (2015) DNA sequence alignment by microhomology sampling during homologous recombination. *Cell*, **160**, 856–869.
13. Harper,J.W. and Elledge,S.J. (2007) The DNA damage response: ten years after. *Mol. Cell*, **28**, 739–745.
14. Giglia-Mari,G., Zotter,A. and Vermeulen,W. (2011) DNA damage response. *Cold Spring Harb. Perspect. Biol.*, **3**, a000745.
15. Shiloh,Y. (2006) The ATM-mediated DNA-damage response: taking shape. *Trends Biochem. Sci.*, **31**, 402–410.
16. Cimprich,K.A. and Cortez,D. (2008) ATR: an essential regulator of genome integrity. *Nat. Rev. Mol. Cell Biol.*, **9**, 616–627.
17. Craven,R.J., Greenwell,P.W., Dominska,M. and Petes,T.D. (2002) Regulation of genome stability by *TEL1* and *MEC1*, yeast homologs of the mammalian ATM and ATR genes. *Genetics*, **161**, 493–507.
18. Kim,S.T., Lim,D.S., Canman,C.E. and Kastan,M.B. (1999) Substrate specificities and identification of putative substrates of ATM kinase family members. *J. Biol. Chem.*, **274**, 37538–37543.
19. Traven,A. and Heierhorst,J. (2005) SQ/TQ cluster domains: concentrated ATM/ATR kinase phosphorylation site regions in DNA-damage-response proteins. *Bioessays*, **27**, 397–407.
20. Cheung,H.C., San Lucas,F.A., Hicks,S., Chang,K., Bertuch,A.A. and Ribes-Zamora,A. (2012) An S/T-Q cluster domain census unveils new putative targets under Tel1/Mec1 control. *BMC Genomics*, **13**, 664.
21. Schwartz,M.F., Duong,J.K., Sun,Z., Morrow,J.S., Pradhan,D. and Stern,D.F. (2002) Rad9 phosphorylation sites couple Rad53 to the *Saccharomyces cerevisiae* DNA damage checkpoint. *Mol. Cell*, **9**, 1055–1065.
22. Lee,S.J., Schwartz,M.F., Duong,J.K. and Stern,D.F. (2003) Rad53 phosphorylation site clusters are important for Rad53 regulation and signaling. *Mol. Cell. Biol.*, **23**, 6300–6314.
23. Chen,S.H., Smolka,M.B. and Zhou,H. (2007) Mechanism of Dun1 activation by Rad53 phosphorylation in *Saccharomyces cerevisiae*. *J. Biol. Chem.*, **282**, 986–995.
24. Carballo,J.A., Johnson,A.L., Sedgwick,S.G. and Cha,R.S. (2008) Phosphorylation of the axial element protein Hop1 by Mec1/Tel1 ensures meiotic interhomolog recombination. *Cell*, **132**, 758–770.
25. Chuang,C.N., Cheng,Y.H. and Wang,T.F. (2012) Mek1 stabilizes Hop1-Thr318 phosphorylation to promote interhomolog recombination and checkpoint responses during yeast meiosis. *Nucleic Acids Res.*, **40**, 11416–11427.
26. Herruzo,E., Ontoso,D., Gonzalez-Arranz,S., Cavero,S., Lechuga,A. and San-Segundo,P.A. (2016) The Pch2 AAA+ ATPase promotes phosphorylation of the Hop1 meiotic checkpoint adaptor in response to synaptonemal complex defects. *Nucleic Acids Res.*, **44**, 7722–7741.
27. Busygina,V., Sehorn,M.G., Shi,I.Y., Tsubouchi,H., Roeder,G.S. and Sung,P. (2008) Hed1 regulates Rad51-mediated recombination via a novel mechanism. *Genes Dev.*, **22**, 786–795.
28. Niu,H., Wan,L., Busygina,V., Kwon,Y., Allen,J.A., Li,X., Kunz,R.C., Kubota,K., Wang,B., Sung,P. *et al.* (2009) Regulation of meiotic recombination via Mek1-mediated Rad54 phosphorylation. *Mol. Cell*, **36**, 393–404.
29. Carballo,J.A. and Cha,R.S. (2007) Meiotic roles of Mec1, a budding yeast homolog of mammalian ATR/ATM. *Chromosome Res.*, **15**, 539–550.
30. Falk,J.E., Chan,A.C., Hoffmann,E. and Hochwagen,A. (2010) A Mec1- and PP4-dependent checkpoint couples centromere pairing to meiotic recombination. *Dev. Cell*, **19**, 599–611.
31. Carballo,J.A., Panizza,S., Serrentino,M.E., Johnson,A.L., Geymonat,M., Borde,V., Klein,F. and Cha,R.S. (2013) Budding yeast ATM/ATR control meiotic double-strand break (DSB) levels by down-regulating Rec114, an essential component of the DSB-machinery. *PLos Genet.*, **9**, e1003545.
32. Cartagena-Lirola,H., Guerini,I., Viscardi,V., Lucchini,G. and Longhese,M.P. (2006) Budding yeast Sae2 is an *in vivo* target of the Mec1 and Tel1 checkpoint kinases during meiosis. *Cell Cycle*, **5**, 1549–1559.
33. Brush,G.S., Clifford,D.M., Marinco,S.M. and Bartrand,A.J. (2001) Replication protein A is sequentially phosphorylated during meiosis. *Nucleic Acids Res.*, **29**, 4808–4817.
34. Cheng,Y.H., Chuang,C.N., Shen,H.J., Lin,F.M. and Wang,T.F. (2013) Three distinct modes of Mec1/ATR and Tel1/ATM activation illustrate differential checkpoint targeting during budding yeast early meiosis. *Mol. Cell. Biol.*, **33**, 3365–3376.
35. Lo,Y.H., Chuang,C.N. and Wang,T.F. (2014) Pch2 prevents Mec1/Tel1-mediated Hop1 phosphorylation occurring independently of Red1 in budding yeast meiosis. *PLoS One*, **9**, e85687.
36. Farmer,S., Hong,E.J., Leung,W.K., Argunhan,B., Terentyev,Y., Humphryes,N., Toyoizumi,H. and Tsubouchi,H. (2012) Budding yeast pch2, a widely conserved meiotic protein, is involved in the initiation of meiotic recombination. *PLoS One*, **7**, e39724.
37. Joshi,N., Brown,M.S., Bishop,D.K. and Borner,G.V. (2015) Gradual implementation of the meiotic recombination program via checkpoint pathways controlled by global DSB levels. *Mol. Cell*, **57**, 797–811.
38. Corcoles-Saez,I., Dong,K., Johnson,A.L., Waskiewicz,E., Costanzo,M., Boone,C. and Cha,R.S. (2018) Essential function of Mec1, the budding yeast ATM/ATR checkpoint-response kinase, in protein homeostasis. *Dev. Cell*, **46**, 495–503.

39. Corcoles-Saez,I., Dong,K. and Cha,R.S. (2019) Versatility of the Mec1(ATM/ATR) signaling network in mediating resistance to replication, genotoxic, and proteotoxic stresses. *Curr. Genet.*, **65**, 657–661.
40. Cheng,C.H., Lo,Y.H., Liang,S.S., Ti,S.C., Lin,F.M., Yeh,C.H., Huang,H.Y. and Wang,T.F. (2006) SUMO modifications control assembly of synaptonemal complex and polycomplex in meiosis of *Saccharomyces cerevisiae*. *Genes Dev.*, **20**, 2067–2081.
41. Lin,F.M., Lai,Y.J., Shen,H.J., Cheng,Y.H. and Wang,T.F. (2010) Yeast axial-element protein, Red1, binds SUMO chains to promote meiotic interhomologue recombination and chromosome synapsis. *EMBO J.*, **29**, 586–596.
42. Ahuja,J.S. and Borner,G.V. (2011) Analysis of meiotic recombination intermediates by two-dimensional gel electrophoresis. *Methods Mol. Biol.*, **745**, 99–116.
43. Shinohara,M., Gasior,S.L., Bishop,D.K. and Shinohara,A. (2000) Tid1/Rdh54 promotes colocalization of Rad51 and Dmc1 during meiotic recombination. *Proc. Natl. Acad. Sci. U.S.A.*, **97**, 10814–10819.
44. Flott,S., Kwon,Y., Pigli,Y.Z., Rice,P.A., Sung,P. and Jackson,S.P. (2011) Regulation of Rad51 function by phosphorylation. *EMBO Rep.*, **12**, 833–839.
45. Chabes,A., Domkin,V. and Thelander,L. (1999) Yeast Sml1, a protein inhibitor of ribonucleotide reductase. *J. Biol. Chem.*, **274**, 36679–36683.
46. Zhao,X., Muller,E.G. and Rothstein,R. (1998) A suppressor of two essential checkpoint genes identifies a novel protein that negatively affects dNTP pools. *Mol. Cell*, **2**, 329–340.
47. Martini,E., Diaz,R.L., Hunter,N. and Keeney,S. (2006) Crossover homeostasis in yeast meiosis. *Cell*, **126**, 285–295.
48. Lao,J.P., Cloud,V., Huang,C.C., Grubb,J., Thacker,D., Lee,C.Y., Dresser,M.E., Hunter,N. and Bishop,D.K. (2013) Meiotic crossover control by concerted action of Rad51-Dmc1 in homolog template bias and robust homeostatic regulation. *PLoS Genet.*, **9**, e1003978.
49. Hunter,N. and Kleckner,N. (2001) The single-end invasion: an asymmetric intermediate at the double-strand break to double-Holliday junction transition of meiotic recombination. *Cell*, **106**, 59–70.
50. Oh,S.D., Jessop,L., Lao,J.P., Allers,T., Lichten,M. and Hunter,N. (2009) Stabilization and electrophoretic analysis of meiotic recombination intermediates in *Saccharomyces cerevisiae*. *Methods Mol. Biol.*, **557**, 209–234.
51. Le Tallec,B., Barrault,M.B., Courbeyrette,R., Guerois,R., Marsolier-Kergoat,M.C. and Peyroche,A. (2007) 20S proteasome assembly is orchestrated by two distinct pairs of chaperones in yeast and in mammals. *Mol. Cell*, **27**, 660–674.
52. Smith,G.C. and Jackson,S.P. (1999) The DNA-dependent protein kinase. *Genes Dev.*, **13**, 916–934.
53. Slater,M.L., Sharrow,S.O. and Gart,J.J. (1977) Cell cycle of *Saccharomyces cerevisiae* in populations growing at different rates. *Proc. Natl. Acad. Sci. U.S.A.*, **74**, 3850–3854.
54. Brewer,B.J., Chlebowicz-Sledziewska,E. and Fangman,W.L. (1984) Cell cycle phases in the unequal mother/daughter cell cycles of *Saccharomyces cerevisiae*. *Mol. Cell. Biol.*, **4**, 2529–2531.
55. Padmore,R., Cao,L. and Kleckner,N. (1991) Temporal comparison of recombination and synaptonemal complex formation during meiosis in *S. cerevisiae*. *Cell*, **66**, 1239–1256.
56. Cha,R.S., Weiner,B.M., Keeney,S., Dekker,J. and Kleckner,N. (2000) Progression of meiotic DNA replication is modulated by interchromosomal interaction proteins, negatively by Spo11p and positively by Rec8p. *Genes Dev.*, **14**, 493–503.
57. Borner,G.V. and Cha,R.S. (2015) Analysis of yeast sporulation efficiency, spore viability, and meiotic recombination on solid medium. *Cold Spring Harb. Protoc.*, **2015**, 1003–1008.
58. Weinert,T.A., Kiser,G.L. and Hartwell,L.H. (1994) Mitotic checkpoint genes in budding yeast and the dependence of mitosis on DNA replication and repair. *Genes Dev.*, **8**, 652–665.
59. Mallory,J.C. and Petes,T.D. (2000) Protein kinase activity of Tel1p and Mec1p, two *Saccharomyces cerevisiae* proteins related to the human ATM protein kinase. *Proc. Natl. Acad. Sci. USA*, **97**, 13749–13754.
60. Ho,B., Baryshnikova,A. and Brown,G.W. (2018) Unification of protein abundance datasets yields a quantitative *Saccharomyces cerevisiae* proteome. *Cell Syst.*, **6**, 192–205.
61. Callan,H.G. (1974) DNA replication in the chromosomes of eukaryotes. *Cold Spring Harb. Symp. Quant. Biol.*, **38**, 195–203.
62. Macossay-Castillo,M., Marvelli,G., Guharoy,M., Jain,A., Kihara,D., Tompa,P. and Wodak,S.J. (2019) The balancing act of intrinsically disordered proteins: enabling functional diversity while minimizing promiscuity. *J. Mol. Biol.*, **431**, 1650–1670.
63. Katoh,K. and Standley,D.M. (2013) MAFFT multiple sequence alignment software version 7: improvements in performance and usability. *Mol. Biol. Evol.*, **30**, 772–780.
64. Beranger,F., Aresta,S., de Gunzburg,J. and Camonis,J. (1997) Getting more from the two-hybrid system: N-terminal fusions to LexA are efficient and sensitive baits for two-hybrid studies. *Nucleic Acids Res.*, **25**, 2035–2036.